

Final Technical Report

Project Title:

Lost Foam Thin Wall: Feasibility of Producing Lost Foam Castings in Aluminum and Magnesium Based Alloys

Award Number: DE-FC36-04GO14230

Project Period (January 2004 - March 31, 2014)

Principal Investigators

Yemi Fasoyinu, 905-645-0779, Yemi.Fasoyinu@NRCan.gc.ca (2004 – 2014)

John A. Griffin, 205-975-8461, jagrif@uab.edu (2012 – 2014)

Recipient Organizations:

CanmetMATERIALS, Natural Resources Canada
183 Longwood Road South, Hamilton, Ontario, L8P 0A5, Canada

Laboratory Former Address:
CANMET MTL (Materials Technology Laboratory), Natural Resources Canada
568 Booth Street, Ottawa, ON, K1A 0G1, Canada

The University of Alabama at Birmingham
Material Science & Engineering Department, 501 12th Street South
501 Building, Room 102, Birmingham, AL 35294-4450, USA

Subtask Participants: (January 2004 – June 30, 2009)

Eck Industries, Inc.
Foseco-Morval, Division of Foseco, Canada
Flow Science Inc.

Subtask Participants: (June 2012 – March 31, 2014)

University of Alabama, Birmingham (UAB), AL, USA
Eck Industries, Inc.

March 2014

Acknowledgment, Disclaimer and Proprietary Data Notice

Acknowledgment: This report is based upon work supported by the U. S. Department of Energy under Award No.DE-FC36-04GO14230

Disclaimer: Any findings, opinions, and conclusions or recommendations expressed in this report are those of the author(s) and do not necessarily reflect the views of the Department of Energy.

Proprietary Data Notice: None in report.

Table of Contents

List of Acronyms	v
List of Figures	v
List of Tables	vi
1 Executive Summary	1
2 Introduction	2
3. Background	4
3.1 Specific Goals and Objectives	6
TASK 1 Selection of Prototype Components	7
TASK 2 Casting Trials at CMAT: 2004-2009	7
TASK 3 Metallography and Mechanical Property Evaluation	7
TASK 4 Casting Trials at UAB: 2012-2014	7
3.2 Team Members	7
4. Results and Discussion	8
4.1 TASK 1: Selection of Prototype Components	8
4.1.1 Widget	8
4.1.2 Box and Plate	9
4.1.3 Intake-Manifold and Elx-Body	9
4.2 TASK 2 Casting Trials at CMAT	10
4.2.1 Phase I: Experimental Details	10
4.2.1.1 Melting and pouring	10
4.2.1.2 Vacuum Box and Manifold System	10
4.2.1.3 Gating System Design	11
4.2.1.4 Pattern Preparation and Molding Media	11
4.2.2 Results and Discussion	14
4.2.2.1 Application of Vacuum	15
4.2.2.2 Gating System Design and Foam Density	16
4.2.2.3 Molding Media	17
4.2.2.4 Metallography and X-Ray Analyses	18
4.2.2.5 Summary and Conclusions	21
4.2.3 Castings Poured from AZ91D and AM50	22
4.2.3.1 Widget Castings Poured from AZ91D Using Hollow Sprue	24
4.2.3.2 Plate, Box, and Widget Castings Poured from AM50	25
4.2.3.3 Analysis of Fold Defects in Box and Widget Castings	26
4.2.3.4 Elx-Body and Intake-Manifold Castings Poured from AZ91D	29
4.2.3.5 Summary and Conclusions	30
4.3 TASK 3 Mechanical Properties and Metallography	31
4.3.1 Experimental	31

4.3.2 Results and Discussion	33
4.3.2.1 Alloy AZ91D, As Cast (F) and Heat Treated (T6)	35
4.3.2.2 Alloy AM50, As Cast (F) and Heat Treated (T6)	35
4.3.2.3 Alloy ZE41, As Cast (F) and Heat Treated (T5)	35
4.3.2.4 Metallography and Microstructure	38
4.3.2.5 Summary and Conclusions	40
Phase II – UAB Casting Trials	41
TASK 4 Casting Trials at UAB	41
4.4.1 Phase II: Experimental	41
4.4.2 Results and Discussion	43
5 Benefits Assessment	58
5.1 Casting Trials at CMAT	58
5.2 Casting Trials at UAB	58
6 Commercialization	59
6.1 Casting Trials at CMAT	59
6.2 Casting Trials at UAB	59
7 Accomplishments	60
7.1 Casting Trials at CMAT	60
7.1.1 Innovative Processing Techniques	60
7.1.2. Publications	60
7.2 Casting Trials at UAB	61
7.2.1 Publications	61
8 Conclusions (CMAT and UAB)	61
8.1 CMAT	61
8.2 UAB	62
9 Recommendations (CMAT and UAB)	62
9.1 CMAT	62
9.2 UAB	63
10 References (CMAT and UAB)	63

List of Acronyms

CMAT	CanmetMATERIALS
UAB	University of Alabama at Birmingham
LFC	Lost Foam Casting
SUP	Solidification Under Pressure
VAP	Vacuum Assisted Pouring

List of Figures

Figure 4.1.1	Photographs of widget foam pattern.	9
Figure 4.1.2	Photographs of (a) box and (b) plate foam patterns.	9
Figure 4.2.1	Vacuum box and pressure manifold system.	11
Figure 4.2.2	Photographs of widget patterns cluster before and after pouring.	12
Figure 4.2.3	Defect-free castings from side-gated castings poured at 730°C. Vacuum was applied during pouring. Alloy AZ91E.	17
Figure 4.2.4	Defect-free castings from top-gated castings poured at 730°C. Vacuum was applied during pouring. Alloy AZ91E.	18
Figure 4.2.5	Castings poured at 730°C without vacuum application. Full castings could not be produced. Alloy AZ91E.	18
Figure 4.2.6	Widget casting showing where samples were removed for metallography.	19
Figure 4.2.7	Microstructures from 25 mm and 5 mm thick sections. Glycol Etch.	20
Figure 4.2.8	X-ray radiography from selected castings using vacuum.	21
Figure 4.2.9	Examples of casting defects on widget castings poured from Mg alloy AZ91D.	23
Figure 4.2.10	Widget castings poured at (a) 725°C and (b) 775°C. The extent of mold filling, casting defects, and surface quality are shown for each of the casting.	24
Figure 4.2.11	24 mm plate casting poured at 720°C from AM50.	26
Figure 4.2.12	Box casting, poured at 760°C from AM50 without vacuum assistance.	27
Figure 4.2.13	Widget castings poured at 760°C from AM50.	27
Figure 4.2.14	Fracture surfaces from box casting poured at 720°C showing fold defects.	27
Figure 4.2.15	SEM of fracture surface from the widget pattern casting showing (a) clean area, and fold defects: (b) oxide film, (c) EDS of (b) and (d) dendritic structure and porosity.	28
Figure 4.2.16	Elx-body and intake-manifold foam casting assembly.	29
Figure 4.2.17	Elx-body showing compaction defect and good surface finish.	29
Figure 4.3.1	Photographs of plate foam clusters of (a) bottom and (b) top gated plate castings.	32
Figure 4.3.2	Sample X-ray of 24 mm thick plate.	32
Figure 4.3.3	Photographs of (a) round and (b) rectangular test bars.	32
Figure 4.3.4	Tensile properties versus plate thickness for AZ91D, AM50 and ZE41A.	36
Figure 4.3.5	Yield strength, ultimate tensile strength, and elongation in the as-cast condition.	37
Figure 4.3.6	Microstructures from AZ91D round test bars machined from 24 mm thick plate.	38
Figure 4.3.7	The BSE of (a) eutectic area and (b) EDS of an inclusion in AZ91D.	38
Figure 4.3.8	Fracture surface of a test bar from AM50 at (a) low and (b) higher magnifications.	39
Figure 4.3.9	EDS spectra from AM50 round test bars machined from 24 mm thick plate.	39
Figure 4.4.2	Vacuum assisted pouring schematic.	44
Figure 4.4.5	Top gated engine block.	46
Figure 4.4.6	Flask showing pouring basin inside pressure vessel.	46
Figure 4.4.7	Engine block showing where test samples were sectioned from.	47

Figure 4.4.8 Effect of VAP and SUP on ultimate strength for alloy A356.	50
Figure 4.4.9 Effect of VAP and SUP on strain at maximum stress for alloy A356.	50
Figure 4.4.10 Porosity of Casting A, A356, 1450°F, VAP (0 psig) and SUP (0 psig), Bearing #4. ...	51
Figure 4.4.11 Porosity of Casting AB, A356, 1250°F, VAP (-4.5 psig) and SUP (0 psig), Bearing #4.	51
.....	51
Figure 4.4.12 Porosity of Casting B, A356, 1250°F, VAP (-4.5 psig) and SUP (150 psig), Bearing #4.	51
.....	51
Figure 4.4.13 Porosity of Casting C, A356, 1450°F, VAP (0 psig) and SUP (150 psig), Bearing #4.	51
Figure 4.4.14 Effect of VAP/SUP on ultimate strength for alloy A206.	52
Figure 4.4.15 Effect of VAP/SUP on strain at maximum stress for alloy A206.	52
Figure 4.4.16 Porosity of Casting D, A206, 1510°F, VAP (0 psig) and SUP (0 psig), Bearing #4. ...	53
Figure 4.4.17 Porosity of Casting E, A206, 1310°F, VAP (-4.5 psig) and SUP (150 psig), Bearing #4.	53
.....	53
Figure 4.4.18 Effect of VAP/SUP on ultimate strength for alloy 535.	54
Figure 4.4.19 Effect of VAP/SUP on strain at maximum stress for alloy 535.	54
Figure 4.4.20 Porosity of Casting F, 535, 1470°F, VAP (0 psig) and SUP (0 psig), Bearing #4.	55
Figure 4.4.21 Porosity of Casting G, 535, 1270°F, VAP (-4.5 psig) and SUP (150 psig), Bearing #4.	55
.....	55
Figure 4.4.22 Effect of VAP/SUP on ultimate strength for alloy 319m.	56
Figure 4.4.23 Effect of VAP/SUP on strain at maximum stress for alloy 319m.	56
Figure 4.4.24 Porosity of Casting H, 319m, 1430°F, VAP (0 psig) and SUP (0psig), Bearing #4.	57
Figure 4.4.25 Porosity of Casting J, 319m, 1230°F, VAP (-4.5 psig) and SUP (150 psig), Bearing #4.	57
.....	57

List of Tables

Table 4.2.1 Foam material type and density	12
Table 4.2.2 Sprue type and material	13
Table 4.2.3 Coatings used for the casting trials	14
Table 4.2.4 Thermophysical properties of CarboAccucast ID40TM.....	14
Table 4.2.5 Chemical analyses from selected AZ91E melts	15
Table 4.2.7 Examples of processing temperatures and casting weight.....	16
Table 4.2.8 Chemical analyses of magnesium alloys AZ91D and AM50.....	23
Table 4.2.9 Gravity and vacuum assisted pouring of the plate patterns	25
Table 4.3.1 Heat treatment procedure for the test bars	33
Table 4.3.2 Chemical composition range and analysis from melts prepared.....	34
Table 4.3.4 Mechanical properties of AM50 (Melt No. N6014).....	35
Table 4.3.5 Mechanical properties of ZE41A (Melt No. N5253).....	35
Table 4.4.1 VAP and SUP test matrix	47
Table 4.4.3 Average tensile properties from test matrix alloys	49
Table 4.4.4 Fracture face percent porosity.....	49

1 Executive Summary

With the increased emphasis on vehicle weight reduction, production of near-net shape components by lost foam casting will make significant inroad into the next-generation of engineering component designs. The lost foam casting process is a cost effective method for producing complex castings using an expandable polystyrene pattern and un-bonded sand. The use of un-bonded molding media in the lost foam process will impose less constraint on the solidifying casting, making hot tearing less prevalent. This is especially true in Al-Mg and Al-Cu alloy systems that are prone to hot tearing when poured in rigid molds partially due to their long freezing range. Some of the unique advantages of using the lost foam casting process are closer dimensional tolerance, higher casting yield, and the elimination of sand cores and binders. Most of the aluminum alloys poured using the lost foam process are based on the Al-Si system. Very limited research work has been performed with Al-Mg and Al-Cu type alloys. With the increased emphasis on vehicle weight reduction, and given the high-strength-to-weight-ratio of magnesium, significant weight savings can be achieved by casting thin-wall (≤ 3 mm) engineering components from both aluminum- and magnesium-base alloys.

Historically, magnesium alloy castings have been used in both military and aerospace applications because of their light weight. Recently, the automotive sector has become one of the fastest growing markets for magnesium alloy castings because their high strength-to-weight ratio leads to weight reduction and improved fuel economy. The majority of cast magnesium automotive components are instrument panels produced using the high-pressure die casting process because it lends itself to high volume production at reduced cost. The American Foundry Society (AFS) and automakers are keen to adapt the traditional gravity sand and permanent-mold casting processes (e.g. gravity tilt pour, low pressure, and lost foam) that are commonly used for aluminum alloys to use with magnesium alloys. For example, successful production of engine blocks and heads and other components for power-train applications – produced by the lost-foam casting (LFC) of magnesium alloys – would lead to significant weight savings.

The feasibility of lost foam casting of three magnesium alloy systems was evaluated: magnesium-aluminum-manganese (Mg-Al-Mn); magnesium-aluminum-zinc-manganese (Mg-Al-Zn-Mn); and magnesium-rare earth metal-zirconium (Mg-RE-Zr). The Mg-Al-Zn-Mn and Mg-Al-Mn alloy systems are typified, respectively, by AZ91D/E and AM50, and are used in automotive and other applications. The Mg-RE-Zr system is typified by ZE41A, and has been used as transmission housing for helicopters. The effects of processing variables on the quality of the castings produced during lost foam casting were established. These variables included gating system design, molding media, type of foam and foam density, type of foam coating, sprue material (foam or pyrolite fiber), sprue type (solid or hollow), casting section thickness, and pouring temperatures. Based on the degree of filling, misruns, and the surface finish of the castings poured, Probead 70 foam pattern – one of the four foam types evaluated – produced the best castings.

The application of modest vacuum (-41 kPa [-6 psi]) during pouring and solidification improved mold filling and reduced casting defects. Of the four coatings evaluated, Styromol 169.23 produced the most complete castings with good surface finish and the sharpest features. Overall, the casting trials show that the lost-foam casting process can be a viable manufacturing route for magnesium alloys AZ91D/E, AM50 and ZE41A. This study provides key fundamental knowledge on the issues encountered that can be expected during the casting of these magnesium alloys and processing parameters required for a successful outcome. Although, there is no commercial foundry in North America is dedicated to the lost-foam casting of magnesium alloys, with sustained future efforts this process can become a commercial reality. The casting trials were successful by using the following innovative processing techniques:

- Carboceramic backing sand instead of silica sand (because it does not react with molten magnesium when un-inhibited);
- lower density foam patterns (to reduce foam decomposition products);
- hollow pyrolite fiber sprue (to improve mold filling); and
- application of vacuum during molding and pouring (to improve the packing of the sand around the foam pattern and improved extraction of mold gasses).

Considering the lost foam casting of alloys A356, A206, 535 and modified 319 at the University of Alabama – Birmingham (UAB), this project has demonstrated that net shape thin-walled engineering components can be cast successfully. Similar to other casting processes, the mechanical properties of lost foam aluminum castings, especially tensile elongation, are degraded by the presence of folds and porosity. The occurrence of folds in lost foam castings is usually associated with lower metal temperatures and chaotic mold filling.

The vacuum assisted pouring (VAP) and application of solidification under pressure (SUP) processes allows for lower pouring temperatures (to minimize hydrogen porosity and volumetric shrinkage without generating folds), provide for efficient removal of liquid pyrolysis products and minimize the effect of gravity on metal head pressure. Significant energy savings can be achieved by pouring at about 1250°F (677°C) instead of 1450°F (788°C) normally used for conventional gravity lost foam casting process. The estimated savings for this temperature reduction is 17 - 19%²⁹. In addition, CO₂ emissions would be significantly reduced³⁰ and melting and holding furnace life would be extended.

For Al-Si alloys (A356 and 319m) Al-Cu alloy (A206) there was no dramatic improvement in tensile properties with VAP/SUP, the fracture surface porosity was reduced to 10% of baseline. This would indicate that other metallurgical factor(s) were dominant or optimization of the melting practice and VAP/SUP processing may give better results. Al-Mg alloy 535 showed the most dramatic improvements in tensile properties, a 70% increase in ultimate strength and 300% increase in strain at maximum stress. This report describes the casting procedures and the effects of VAP and SUP on tensile properties and porosity formation during lost foam casting of aluminum alloys A356, A206, 319m and 535.

2 Introduction

With the dramatically increased emphasis on vehicle weight reduction, production of near-net shape components by lost foam casting will make significant inroad into the next-generation of engineering component designs. Already several automotive components are being produced in aluminum base alloys, and some of the automakers are planning to increase the use of magnesium from the current 4 kg per vehicle to about 100 kg by 2020. It is anticipated that the development of viable and economic lost foam casting technique and the use of vacuum technique should result in improved casting quality.

Light alloys based on aluminum and magnesium systems are steadily improving their market share as structural components for transportation and military applications. The lost foam casting process is a cost effective method for producing complex castings using an expandable polystyrene pattern and un-bonded sand. The use of un-bonded molding media in the lost foam process will impose less constraint on the solidifying casting, making hot tearing less prevalent. This is especially true in Al-Mg and Al-Cu alloy systems that are prone to hot tearing when poured in rigid molds due to their long freezing range. Some of the unique advantages of using the lost foam casting process are closer dimensional tolerance, higher casting yield, and the elimination of sand cores and binders. Most of the aluminum alloys poured using the lost foam process are based on the Al-Si system. Very limited work has been done with Al-Mg and Al-Cu type alloys. Many of the magnesium components are currently produced by green sand and high-

pressure die casting processes requiring the use of cores and feeders to ensure defect free castings. It is noted that lost foam casting of magnesium alloys is not yet a commercial reality.

With the increased emphasis on vehicle weight reduction, and given the high-strength-to-weight-ratio of magnesium, significant weight savings can be achieved by casting thin-wall (≤ 3 mm) engineering components from both aluminum- and magnesium-base alloys. The American Foundry Society (AFS) and the automakers are keen on developing the traditional gravity lost foam casting process for magnesium-base alloys. The successful completion of this project should improve the market share of components produced using the lost foam casting process.

CANMET-Materials Technology Laboratory has been involved with R&D on the lost foam casting of aluminum and ductile cast iron castings for a number of years¹⁻⁴. The vacuum-assisted molding and pouring techniques developed at CANMET- MTL have been shown to be an effective way to improve casting quality of aluminum base alloys¹⁻³. It was demonstrated that the vacuum assisted molding and pouring techniques facilitate good packing of the backing sand, improve mold filling (faster, thinner sections, etc.), and extract mold gasses. It was also shown that the lustrous carbon defect observed in the brake caliper and the manifold castings produced from ductile iron melts for GMC was eliminated by the application of vacuum during the lost foam casting process⁴. Other investigators have also discussed the advantages of the application of vacuum during metal casting operations⁵⁻⁷. Some of the advantages of vacuum pouring include ability to produce thin-wall, near-net shape components with complex casting geometry with improved performance. This project focused on magnesium alloys AZ91D/E, AM50, ZE41A and aluminum alloys A535 and A206.

Askeland et al⁸⁻¹¹ provided some guidelines and recommendations on gating system design and casting geometry during the lost foam casting process. The pattern and gating system were produced from expanded polystyrene (EPS) with nominal densities of 1.4 lb/ft³ and 1.6 lb/ft³ respectively. The plate castings produced were 3/16 inch thick (4.8mm). They reported that the size of the gating system had little effect on mold filling and metal velocity in lost foam casting process. However, lower foam density and higher coating permeability resulted in higher fill velocity. A critical velocity of 2.3 cm/s was reported to be beneficial to preclude the formation of porosity defects induced by foam inclusion⁸. They noted that the significance of the sprue, runner and in-gate design is related to the control and removal of foam decomposition products during mold filling. The removal of foam decomposition products through proper gating system design influences the formation of casting defects in lost foam casting. These research results provide some basis for the foam pattern gating system design for thin-wall castings. High coating permeability is sometimes associated with folds and metal penetration during the casting of aluminum alloys¹². For this reason, a low permeability coating may be preferred for aluminum alloys. Higher pouring temperatures may reduce any problems with solidification shrinkage and misruns, especially in thin-wall castings that used the low permeability coating¹³. The effect of metal velocity on defect formation has also been studied¹⁴. It was shown that there is a critical metal velocity window within which casting parameters must be adjusted to assure the production of good quality castings. The formation of internal porosity, folds, surface (orange peel, or carbon) defects, and metal penetration can occur outside this critical velocity window. Recently, a joint research effort by AFS Magnesium and Lost Foam Divisions carried out at Eck Industries Inc., Manitowoc, WI, had demonstrated the viability of lost foam casting of magnesium alloy AZ91E¹⁵. They associated the success of their casting trial to the use of relatively high metal superheat and hollow fiber sprue.

The vacuum assisted pouring (VAP) and application of solidification under pressure (SUP) processes allows for lower pouring temperatures (to minimize hydrogen porosity and volumetric shrinkage without

generating folds), provide for efficient removal of liquid pyrolysis products and minimize the effect of gravity on metal head pressure. Energy savings at pouring temperatures of 1250°F (677°C) compared to 1450°F (788°C) are very large. The estimated savings for this temperature reduction is 17 - 19%²⁹. In addition, CO₂ emissions would be significantly reduced³⁰ and melting and holding furnace life would be extended. Furthermore, the use of non-traditional higher strength aluminum alloys would allow designers to produce either lighter weight components at current stress levels or higher performance parts at current part weight. This would provide significant indirect energy savings and CO₂ emission reduction. Application of SUP at a pressure of 150 psig (1.03 MPa) on A356 and A206 revealed a significant increase in tensile elongation and ultimate strength^{34,35}. Solidification under pressure provides two benefits. The applied pressure will push liquid metal through interdendritic regions with a higher solid fraction compared to a conventionally cast part. This will reduce or eliminate solidification shrinkage in marginally fed sections of a casting. Second, hydrogen porosity volume will be reduced to about one-tenth (at 150 psig) of an atmospheric pour.

3. Background

The use of foam patterns to produce castings was patented almost 50 years ago by Shroyer¹⁶, and variants of the original invention have been used successfully to produce engineering components from both ferrous and non-ferrous alloys. The lost-foam casting (LFC) process is a cost-effective method for producing complex castings using an expandable polystyrene pattern and unbonded sand. The fundamental steps of the lost-foam casting process consist of making a polystyrene foam pattern and its gating system, providing a refractory-coating on the pattern and placing it in a flask, surrounding it by unbonded sand, and vibrating it to achieve maximum compaction of the sand around the foam pattern assembly making the complete mold. Molten metal is poured directly on the top of the coated gating system. The heat from the melt serves to vaporize the polystyrene pattern leaving a casting that is a replica of the foam pattern. The gases that form during the vaporization of the pattern permeate through the coating and sand and exit through the flask vents.

Some unique advantages of the lost foam casting process are close dimensional tolerance, part consolidation, high casting yield, capability to produce complex castings, and elimination of sand cores and binders. The flexibility of gluing foam sections together to form one component with complex internal passages – as in engine blocks and heads – without the use of cores common in the sand-casting process is one of the major advantages of the LFC process. Some automotive engine blocks and heads are cast from aluminum alloy A356 using the LFC process¹⁷. It is quite possible that some of the new magnesium alloys developed for high-temperature applications could be used in the same way with further reduction in vehicle weight and improvement in fuel economy.

High coating permeability can sometimes lead to the formation of fold defects and metal penetration during the casting of aluminum alloys¹². High pouring temperatures may reduce many problems associated with solidification such as shrinkage and misruns, especially in thin-wall castings that used low-permeability coatings¹³. Many years of research at the University of Alabama (UAB) have generated very useful lost-foam casting processing data for aluminum and iron castings¹⁸.

Magnesium Division 6 of the AFS published the “Magnesium Casting Industry Technology Roadmap” that outlines the strategic technology agenda for achieving the needs and expectations of the industry and

its customers¹⁹. One of the key components of the roadmap is to develop advanced process technologies to improve affordability and competitiveness of magnesium cast components in all markets that value lightweight performance metals. The need to develop new magnesium casting processes such as gravity and low-pressure permanent-mold casting as well as lost-foam casting was emphasized in this publication. The automotive market is one of the fastest growing magnesium markets due largely to its high strength-to-weight ratio and the interest in reducing vehicle weight to improve fuel efficiency.

Three magnesium alloy systems – magnesium-aluminum-manganese (Mg-Al-Mn), magnesium-aluminum-zinc-manganese (Mg-Al-Zn-Mn), and magnesium-rare earth metal-zirconium (Mg-RE-Zr) – were evaluated in this study. The Mg-Al-Zn-Mn and Mg-Al-Mn alloy systems typified by AZ91D/E and AM50/60 are used in automotive applications and usually cast by gravity sand, and permanent mold (e.g. gravity tilt pour, low pressure, and high pressure) casting processes. The Mg-RE-Zr system is typified by ZE41A and is used as sand castings in transmission housing for helicopters. Most magnesium automotive components, such as instrument panels, are produced by the high-pressure die casting process because it lends itself to high volume production at relatively low cost. Some automotive components are not practical to produce by die casting for many reasons. Many of the magnesium casting alloys that could be used in engineering applications are subject to hot tearing, particularly when parts are constrained in a metal or sand mold during solidification. For example, some of the high-temperature and creep-resistant magnesium alloys are prone to hot tearing when poured in metal molds. The use of un-bonded sand in the lost-foam process should reduce constraint during solidification and thus reduce the tendency to hot tearing.

Some of the major considerations for the lost-foam casting of magnesium alloys compared with that of aluminum alloys are the lower heat content and higher chemical reactivity of magnesium. Due to the low thermal heat content, the filling of a lost-foam mold can present a great challenge. Given that the specific heat of molten aluminum is higher than that of magnesium, a low-conductivity media with low thermal expansion properties would be preferred for magnesium alloys. Another unique factor for magnesium is that it reacts with silica sand, commonly used for aluminum alloys as a backing material. Therefore, the use of a sand inhibitor such as a mixture of sulfur and potassium fluoroborate is usually mixed with silica sand to decrease the possibility of reaction between the sand and the molten magnesium.

A significant number of the R&D activities on LFC of magnesium alloys that are in the public domain are occurring in China, Germany, USA, and Canada²⁰. The main focus of these activities is related to LFC process control to improve mold filling and surface finish, and eliminate surface defects such as burned-on sand, misruns, folds, and poor surface finish. The application of vacuum during conventional gravity lost-foam casting and the use of low pressure (counter gravity) are the principal processes that are being developed. Some limited studies on mechanical and corrosion properties of selected magnesium alloys have also been undertaken. The foam components used in the various studies are small in size with either simple or relatively complex geometry. The removal of the pyrolysis product during foam pattern degradation is one of the major issues with respect to magnesium lost-foam casting because of its low heat content. Despite these efforts, lost-foam casting of magnesium alloys is not yet a commercial reality. The AFS and automakers are keen on developing the traditional gravity lost foam casting process for magnesium alloys. This report presents the results of our study of the effects of molding media, foam coating, and the use of hollow sprue on the casting of selected magnesium alloys.

Similar to other casting processes, tensile mechanical properties of lost foam aluminum castings, especially tensile elongation, are degraded by the presence of folds and porosity. The root cause of folds has been traced to merging metal fronts contaminated with residual pyrolysis products and aluminum

oxide^{26, 27}. The occurrence of folds in lost foam castings is usually associated with lower metal temperatures and chaotic mold filling. Lower metal temperatures are usually found in last areas to fill. Chaotic metal filling can be caused by high momentum early in the filling process or “fingering” at the metal front later in filling due to varying pattern permeability²⁷. Timely removal of the pyrolysis products is vital to producing castings with a minimum of folds. Evidence of the residual pyrolysis products can be observed on casting surfaces as brown traces. Typical foundry remedies for reducing fold occurrence are increased pouring temperature, patterns that include “no fold” beads, gating changes and pattern geometry changes. A higher pouring temperature has historically been the most common and least expensive remedy; however, higher temperature increases hydrogen solubility and solidification shrinkage. Porosity in lost foam aluminum castings can be traced to three major sources – hydrogen gas, solidification shrinkage, and entrapped pyrolysis gases. Hydrogen concentration can be controlled with de-gassing. Porosity formed by pyrolysis gases is usually addressed by coating selection and pouring temperature. Solidification shrinkage can be managed with gating to feed critical areas or with risers if necessary.

Gravity filling generates metal head pressure gradients in relatively large castings and multiple layered castings in the flask. These pressure gradients generate higher metal velocities near the drag surface and lower metal velocities near the cope. This is not a major issue with open cavity processes due to higher overall metal velocities; however, the lower metal velocities in LFC cause significant temperature gradients which affect metal feeding during filling and solidification. Coatings and pouring temperatures are adjusted to minimize casting anomalies that occur in the areas last to fill (lowest temperatures). Anomalies are typically folds, which form when insufficient time is available for the pyrolysis products to exit the casting cavity before solidification. Typically, the foundry solution is higher pouring temperatures.

3.1 Specific Goals and Objectives

The key objectives of the research program were to: (a) develop appropriate lost foam casting technology for near-net shape prototype engineering components from selected magnesium and aluminum alloys, and (b) investigate the effects of vacuum molding and pouring techniques on the quality of prototype thin-wall components produced during lost foam casting.

The focus of the experimental program from 2004 to 2009 at CanmetMATERIALS was magnesium alloys. To this end, the experimental program focused on the feasibility of lost foam casting of magnesium alloy AZ91E and the casting of prototype components from magnesium alloys AZ91D and AM50 and this was followed by the evaluation of mechanical properties of magnesium alloys AZ91, AM50 and ZE41 determined from plate castings.

The focus of the experimental program from 2012 to 2013 at University of Alabama at Birmingham (UAB) was the hot tear susceptible aluminum alloys 206 and 535. The component selected for the casting trials was an engine block (GM ETEC). The effects of vacuum assisted pouring (VAP) and solidification under pressure (SUP) on the casting properties during lost foam casting was evaluated. Previous research within the Lost Foam Consortium at UAB has shown that VAP and SUP can individually reduce porosity in A319 and 356 aluminum engine block castings. This reduction in porosity results in increased ductility (% elongation) which indicates a significant increase in fatigue strength. The project objectives were met by conducting experiments as described in the tasks below.

TASK 1 Selection of Prototype Components

In consultation with AFS and industry partners lost foam prototype components for use in automotive, marine, and other applications were selected for the experimental program. Some of the key considerations in the selection of the foam patterns were casting geometry its section thickness.

TASK 2 Casting Trials at CMAT: 2004-2009

The key focus of the casting trials at CanmetMATERIALS (CMAT) from 2004 to 2009 was to evaluate the effect of the processing conditions on the casting and solidification of selected magnesium alloys. The effects of foam density, foam pattern material, and foam coating, and number of castings per cluster were evaluated. Some new foam beads and/or improved foam pattern material were tried during the casting trials. The effect of molding media such as silica sand and a synthetic mullite and use of sand inhibitor were investigated for magnesium alloys. The effects of gating system design and location ingate (top, side and bottom) on mold filling was investigated. The application of vacuum during molding and solidification of the lost foam castings was investigated. A vacuum molding box and manifold equipment for vacuum application were fabricated from mild steel. The level of vacuum needed for molding, filling, and extraction of generated gases during casting solidification was determined.

TASK 3 Metallography and Mechanical Property Evaluation

Selected castings in the cluster were X-rayed to evaluate casting soundness. Samples were sectioning from castings poured for metallography, fold tests, and other defect characterization. Microstructural characterization of sectioned test samples using optical metallography techniques was completed. For evaluation of mechanical properties, test samples were machined from plate castings with different thicknesses and the tensile properties (UTS, YS, and % elongation) were determined.

TASK 4 Casting Trials at UAB: 2012-2014

The key focus of the casting trials at UAB from June 2012 to March 31, 2014 was to evaluate the effects of vacuum assisted pouring (VAP) and solidification under pressure (SUP) during lost foam casting of hot tear susceptible aluminum alloys 206 and 535. The component selected for the casting trials was an engine block component. The effects of VAP and SUP on the casting properties during lost foam casting were evaluated. The mechanical properties and relative porosity of samples sectioned from different part of the engine block casting was determined.

3.2 Team Members

Dr. Yemi Fasoyinu is the principal investigator and project leader from January 2004 to March 31, 2014. He created the project proposal in 2004 with contributions from Dr. Mahi Sahoo (now retired). With support personnel from CanmetMATERIALS (CMAT) Experimental Casting Laboratory and industry partners he was responsible for the delivery of the project from 2004 to 2014. He provided the scientific leadership in the selection of unique processing equipment and materials that includes the design and fabrication of a steel vacuum box and its manifold system and the training of project team. The key focus of the casting trials from 2004 to 2009 was selected magnesium alloys. The key focus of the casting trials from June 2012 to March 31, 2014 were aluminum alloys 206 and 535.

CanmetMATERIALS team: Experimental casting laboratory personnel, mechanical testing, metallography and microstructure evaluation, and NDT evaluation.

University of Alabama at Birmingham (UAB) team: Dr. John Griffin, and others evaluated the effects of vacuum assisted pouring (VAP) and solidification under pressure (SUP) during the casting of an engine block casting by lost foam casting process from aluminum alloys 206 and 535. UAB has shown in their previous studies that VAP and SUP can individually reduce porosity in A319 and A356 aluminum engine block castings.

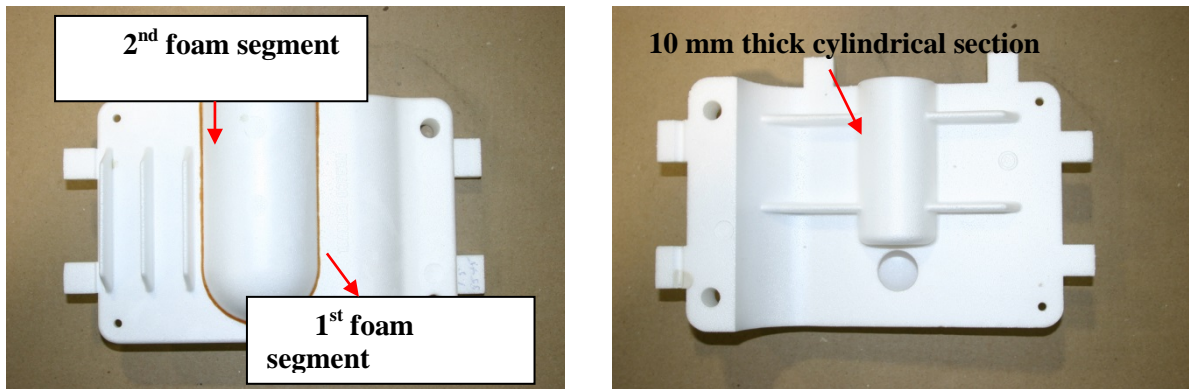
4. Results and Discussion

4.1 TASK 1: Selection of Prototype Components

Six foam pattern types were selected for the casting trials at CanmetMATERIALS (CMAT) Experimental Casting Laboratory (ECL) and one at University of Alabama Birmingham (UAB). The Widget, Box, Plate, Elx-body, and Intake manifold patterns were evaluated using selected magnesium alloys in Phase I studies at CMAT. The engine block pattern was evaluated in Phase II at UAB for selected aluminum alloys.

4.1.1 Widget

The expandable polystyrene (EPS) widget foam pattern is made up of two foam segments. Photographs of a widget foam pattern are shown in Figures 4.1.1 (a) and (b) respectively. The foam densities evaluated were 0.021 and 0.026 g/cm³ (1.3 and 1.6 lb/ft³). The nominal pattern dimensions were 150 mm (6 in.) in height, 220 mm (8.7 in.) in width, and the thickness varied from 5 mm (0.20 in.) to 25 mm (1.0 in.). In addition, there were three vertical ribs 2 mm (0.08 in.) thick, 8 mm (0.32 in.) in height and 85 mm (3.346 in.) in length on one side, and four horizontal ribs, each about 3 mm (0.12 in.) in thickness, 45 mm (1.77 in.) in length and 12 mm (0.47 in.) in width on the other side. These horizontal ribs connected to a central cylindrical section 5 mm (0.20 in.) thick, and 40 mm (1.57 in.) diameter. The dimensions of each of the two side ingates at the thicker end (25 mm) and thinner end (5 mm) are 24 x 10 mm (0.94 x 0.39 in.) and 18 x 8 mm (0.71 x 0.31 in.), respectively. In some cases, a riser 24 x 24 mm (0.94 x 0.94 in.) and 60 mm (2.36 in.) in height was attached to the top of the 25 mm (1 in.) thick section of the foam pattern. The foam pattern and its gating systems were dipped in a water-based refractory Styromol 169.2 coating with a specific gravity of 1.36, and hung to dry in air for 24 h or longer before use. The StyromolTM 169.2 foam coating – a high-permeability and high-insulation coating commonly used for aluminum-base alloys – was the only coating used in this work. The estimated thickness of the coating layer after drying ranged from 0.2 to 0.4 mm (0.008 to 0.016 in.). The molding media used in this investigation were silica sand with 50 AFS GFN (Grain Fineness Number) and CarboAccucast-ID40TM, a synthetic mullite with 39 AFS GFN.

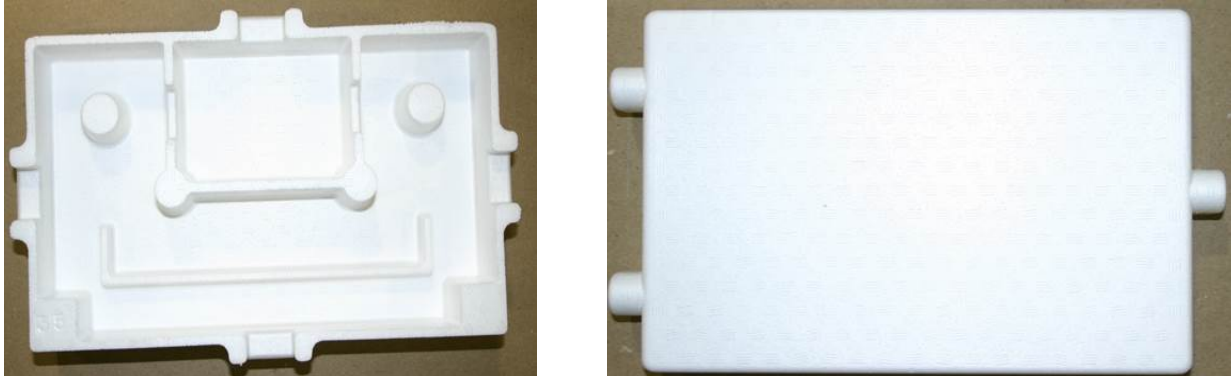


(a) Side 1 with 3, 2 mm thick vertical ribs. (b) Side 2 with 4, 3 mm thick horizontal ribs.

Figure 4.1.1 Photographs of widget foam pattern.

4.1.2 Box and Plate

The nominal dimensions of the box pattern were 254 mm (10 in.) wide and 152 mm (6 in.) high, and its section thickness varied from 4 to 25 mm (0.16 to 1 in). The nominal dimensions of the foam plate patterns were 203 mm (8 in.) wide and 152 mm (6 in.) high, in three thicknesses: 12, 16 and 24 mm (0.47, 0.63, and 0.94 in.). The nominal density of the box and plate patterns was 0.024 g/cm^3 (1.5 lb/ft^3). Two of the pre-molded ingates in the sprue pattern were glued to the two pre-molded ingates on the plate patterns, and the three pre-molded ingates on the sprue were glued to the side of the box pattern.



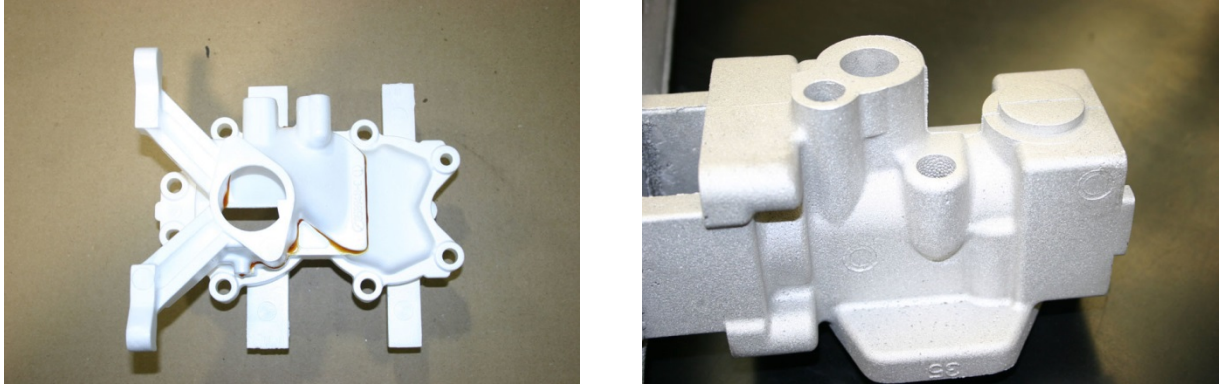
(a) Box.

(b) Plate.

Figure 4.1.2 Photographs of (a) box and (b) plate foam patterns.

4.1.3 Intake-Manifold and Elx-Body

The intake-manifold and elx-body foam patterns are production components normally poured from aluminum alloys using lost foam casting process. Photographs of these patterns are shown in Figures 4.1.3(a) and (b) respectively.



(a) Intake-manifold.

(b) Elx-body.

Figure 4.1.3 Photographs of (a) intake-manifold and (b) Elx-body foam patterns.

4.2 TASK 2 Casting Trials at CMAT

The key focus of the casting trials at CanmetMATERIALS (CMAT) from 2004 to 2009 was to evaluate the effect of the processing conditions described on the casting and solidification of selected magnesium alloys. The effects of foam density, foam pattern material, and foam coating, were evaluated. Some new foam beads and/or improved foam pattern material were tried during the casting trials. The effect of molding media such as silica sand and a synthetic mullite and use of sand inhibitor were investigated for magnesium alloys. The effects of gating system design and location ingate (top, side and bottom) on mold filling was investigated. The effects of foam density, foam coating, number of castings per cluster were also evaluated. The application of vacuum during molding and solidification of the lost foam castings was investigated. A vacuum molding box and manifold equipment for vacuum application were fabricated from mild steel. The level of vacuum needed for molding, filling, and extraction of generated gases during casting solidification was determined.

4.2.1 Phase I: Experimental Details

4.2.1.1 Melting and pouring

Ingots of commercial alloys AZ91D/E and AM50 were melted in a mild steel crucible, using a resistance furnace. The charge size ranged from 12 to 60 kg. The molten magnesium protected by 0.5% sulfur hexafluoride (SF_6) in CO_2 gas as cover gas – a standard melting practice for magnesium and its alloys. The metal was heated to 700°C (1292°F) and degassed for 10 min with argon gas, and test samples were obtained for spectrographic chemical analysis.

The pouring spoon was preheated under a gas flame to reduce temperature drop during pouring. The effect of pouring temperature on filling and casting quality was evaluated using the top gating system design and a gating ratio 1.8:1.8:1. The pouring temperatures evaluated ranged from $720\text{--}780^\circ\text{C}$ ($1328\text{--}1436^\circ\text{F}$). Details on the expandable polystyrene (EPS) widget foam pattern and its photograph are covered in Task 1. Photograph of a widget foam pattern are shown in Figures 4.1.1 (a) and (b) respectively.

4.2.1.2 Vacuum Box and Manifold System

A vacuum box and manifold pressure system were designed and fabricated from mild steel for the casting trials. The dimensions of the box were 508 x 305 x 406 mm (20 x 12 x 16 in.). The foam patterns and their gating system were coated and placed in the molding flasks, half filled with the molding media, and vibrated as more sand was added until the flasks were filled. For the vacuum-assisted casting trials, the vacuum box was covered with a flexible plastic sheet and taped to the side of the flask to prevent vacuum leak during the pouring operation. Vacuum was applied during pouring. Attempts were made to establish the level of vacuum required for mold filling and extraction of gases during casting trials. The applied vacuum varied from -70 to -80 kPa (-10.15 to -11.6 psi). Some castings were also poured without the application of vacuum. A photograph showing the vacuum box and the manifold pressure system is shown in Figure 4.2.1



Figure 4.2.1 Vacuum box and pressure manifold system.

4.2.1.3 Gating System Design

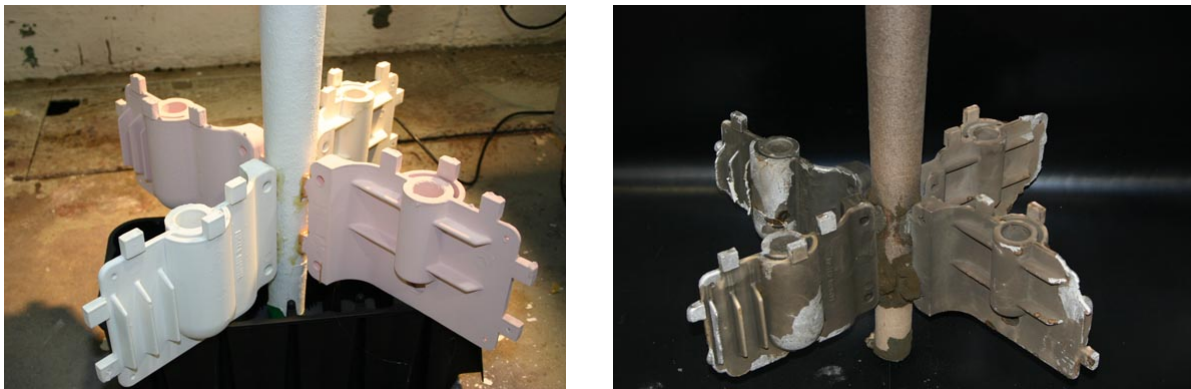
The effects of gating system design (runner, top, side, and bottom ingate design) on mold filling and casting quality for the widget pattern were investigated, as was the concept of a gating ratio (sprue base or choke area: runner area: ingate area) commonly used in open-cavity-mold. Two rectangular solid sprues with dimensions 18 x 18 mm (0.71 x 0.71 in.) and 24 x 24 mm (0.94 x 0.94 in.) were used for the casting trials. The dimensions of the two top ingates and two side ingates were fixed at 9 x 18 mm (0.31 x 0.71 in.) and 12 x 24 mm (0.47 x 0.94 in.), respectively. The lengths of the sprues for the top and side gating designs were 100 mm (4 in.) and 270 mm (10.6 in.), respectively. Two runners, (0.71 x 0.71 in.) and 24 x 24 mm (0.94 x 0.94 in.), were used for the top gating design. There was no runner system for the side-gating design as the sprue was glued directly to the ingates connected to the thicker section of the foam pattern.

4.2.1.4 Pattern Preparation and Molding Media

The dimensions of each of the two side ingates at the thicker end (25 mm) and thinner end (5 mm) were 24 x 10 mm and 18 x 8 mm, respectively. Photographs of the widget pattern are shown in Figures 4.1.1(a) and 1(b). The dimensions of the two pre-molded side ingates of the widget were 12 x 24 mm (0.47 x 0.94 in.). The sprue was glued to the ingates on the thicker section of the foam pattern. The pre-molded ingates on the widget patterns were inserted and glued into rectangular holes cut in the hollow fiber sprue. Four types of foam widget patterns – Brominated EPS, regular EPS, Probead 30 and Probead 70 – were evaluated for magnesium alloy AZ91D. The nominal densities of the Brominated and regular

EPS patterns were 0.026 g/cm^3 (1.6 lb/ft^3) and 0.024 g/cm^3 (1.5 lb/ft^3) for both Probead 30 and Probead 70 foam patterns.

The nominal dimensions of the box pattern were 254 mm (10 in.) wide and 152 mm (6 in.) high, and its section thickness varied from 4 to 25 mm (0.16 to 1 in.). The nominal dimensions of the foam plate patterns were 203 mm (8 in.) wide and 152 mm (6 in.) high, in three thicknesses: 12, 16 and 24 mm (0.47, 0.63, and 0.94 in.). The nominal density of the box and plate patterns was 0.024 g/cm^3 (1.5 lb/ft^3). Two of the pre-molded ingates in the sprue pattern were glued to the two pre-molded ingates on the plate patterns, and the three pre-molded ingates on the sprue were glued to the side of the box pattern. The tapered pyrolite hollow fiber sprue was 88.9 cm (35 in.) in height, 0.64 cm (0.25 in.) thick, and 14 cm (5.5 in.) in diameter at the top and 3.18 cm (1.25 in.) at the bottom. The hollow fiber sprue should improve mold filling in relation to the solid EPS sprue as less foam decomposition products need to be removed and consequently fewer defects should occur. Photographs of widget patterns glued to the hollow fiber sprue (not coated) and the castings produced from them are shown in Figures 4.2.2(a) and (b). Photographs of foam Elx-body and Intake manifold patterns are shown in Figures 4.1.3(a) and (b). The two patterns are production components currently poured from aluminum alloys by a lost-foam production foundry. The two patterns were poured from magnesium alloy AZ91D using a conventional lost foam casting process without vacuum assistance with a hollow EPS sprue. All the foam patterns were side gated. Details on type of foam pattern, sprues, foam pattern density and the castings poured are given in Tables 4.2.1 and 4.2.2.



(a) Widget patterns glued to hollow sprue. (b) Widget castings after pouring.

Figure 4.2.2 Photographs of widget patterns cluster before and after pouring.

Table 4.2.1 Foam material type and density

Foam Reference*	Foam type	Foam casting	Foam density	
			(g/cm^3)	(lb/ft^3)
E	EPS	Widget	0.026	1.6
B	EPS-Brominated	Widget	0.026	1.6
P3	EPS-30%PMMA (Probead 30)	Widget	0.024	1.5
P7	EPS-70%PMMA (Probead 70)	Widget	0.024	1.5
	EPS	Plate	0.024	1.5
	EPS	Box	0.024	1.5
	EPS	Elx-body	0.026	1.6
	EPS	Intake-manifold	0.026	1.6

*identifies the type of foam.

Table 4.2.2 Sprue type and material

Sprue type	Description	Dimensions (cm)
Hollow fiber	Alumina silicate Pyrolite pouring cone	Top diameter: 14 Bottom diameter: 3.2 Height: 89
Foam	Two-part semi-hollow EPS Density: : 0.024 g/cm ³ (1.5 lb/ft ³)	Top diameter: 4 Bottom: 2.54 x 3.2 Height: 53
Foam	Hollow Density: 0.026 g/cm ³ (1.6 lb/ft ³)	Top dimension: 7.6x7.6 Bottom: 5 x 5, with 3.5 hole Height: 79

Four foam coatings (Styromol 140.31, Styromol 169.23, Sempocperm M66L, and Sempocperm M70) were used for the casting trials. All four coatings were used for alloy AZ91D, but only Styromol 169.23 was used for alloy AM50. Styromol coatings 140.31 and 169.23 are generally used for aluminum alloys and the Sempocperm coatings for iron castings. The permeability of Styromol 169.23 and Sempocperm 66L coatings was determined by a Permeter. The average permeability of Styromol 169.23 at 1300 cp viscosity was 8.0, and that of Sempocperm 66L at 1350 cp viscosity was 66. The specifications of the manufacturer are 10-15 and 40-50, respectively. The difference between our measurement and the standard may be due to the direct permeability (fixed volume) method used in the study, rather than the indirect (back pressure) method used in our study. To the authors' knowledge, there is no commercially available coating for lost-foam cast magnesium alloys. The assembled foam patterns were dipped in the appropriate water-based refractory coating and hung to dry in air for 24 to 48 h before use. The estimated coating thickness after drying varied from 0.13 to 0.20 mm (0.005 to 0.008 in.). It is noted that Styromol 169.23 was the only coating used for the Elx-body and Intake manifold patterns. The physical and thermal properties of these coatings are given in Table 4.2.3.

The backing sand for the patterns was CarboAccucast-ID40TM, a synthetic mullite with 40 AFS GFN. The physical and thermal properties of the backing sand are summarized in Table 4.2.4. This molding media is selected for its low thermal expansion, high flowability, and high permeability. The coated foam patterns and gating system were placed in the molding flask; half filled with the molding media, and vibrated as more sand was added until the flasks were filled. For the vacuum assisted casting trials, the vacuum box was covered with a flexible plastic sheet which was taped to the side of the flask to prevent vacuum leakage during pouring. The applied vacuum was -40 kPa (- 6 psi). The vacuum application during the casting trial was for magnesium alloy AM50. Some castings were also poured from AM50 without vacuum assistance using only solid sprues. The hollow fiber sprue was used for two melts of alloy AZ91D without the application of vacuum.

The fold defects from the widget and box castings poured from alloy AM50 at 720°C (100°C superheat) were analyzed; selected castings were broken and the fractured surfaces examined for fold defects. Limited analysis of the oxide and folds defects was performed by examining the fracture surface of the widget casting by scanning-electron microscope (SEM).

Table 4.2.3 Coatings used for the casting trials

Coating reference*	Type of coating	Material	Usage description	Specified permeability (measured)**	Specified viscosity c.p. (measured)**
A	Styromol 169.23	Mica based	Standard coating for aluminum casting with high insulating and high permeability	10-15 (8.0)	1300 (1300)
B	Semcoperm M66L	Alumino-silicate kaolin refractory	Medium permeability for iron casting	40-50 (66)	1300(1350)
C	Semcoperm M70	Alumino-silicate kaolin refractory	High permeability for iron casting	60-70 (-)	1300(990)
D	Styromol 140.31	Silica based	Medium insulating and low permeability for aluminum casting.	2-4 (-)	1300(1310)

*identifies the types of coating; ** Values in bracket were measured.

Table 4.2.4 Thermophysical properties of CarboAccucast ID40TM

Properties	Value
Bulk Density (g/cm ³)	1.81
AFS GFN	40
Thermal Expansion (% Linear Change)	0.65
Thermal Conductivity (cal/h-cm-C)	0.0066
Thermal Heat Capacity (W-s/gm-C)	1.142
Thermal Diffusivity (cm ² /s)	0.0028
Permeability	419

4.2.2 Results and Discussion

The chemical analysis from eleven melts shown in Table 4.2.5. The composition generally falls within the levels recommended for this alloy.

The castings were examined visually for surface defects after removal from the un-bonded molding media. The gating system dimensions, foam density, and coating thickness summarized in Table 4.2.6. The pouring time, calculated gating ratios, pouring temperature, and casting yield from selected melts given in Table 4.2.7. Additional details are given and discussed in the section on metallography.

Table 4.2.5 Chemical analyses from selected AZ91E melts

Melt No.	Composition (Wt. %)						
	Mg	Al	Zn	Mn	Fe	Cu	Ni
ASM	Bal	8.1-9.3	0.4-1.0	0.17-0.35	0.005 max	0.015 max	0.0010 max
N4039	Bal	8.7	0.84	0.18	0.004	0.005	0.0012
N4070	Bal	8.7	0.86	0.21	0.003	0.003	0.0013
N4080	Bal	9.0	0.88	0.20	0.003	–	–
N4086	Bal	8.9	0.87	0.21	0.002	–	0.001
N4087	Bal	8.8	0.79	0.21	0.002	0.01	0.001
N4108	Bal	8.8	0.83	0.21	0.001	0.008	0.001
N4121	Bal	8.9	0.80	0.24	0.001	0.009	0.001
N4127	Bal	8.6	0.81	0.21	0.001	0.008	0.001
N4136	Bal	8.7	0.82	0.22	0.001	0.010	0.001
N4137	Bal	8.8	0.79	0.20	0.001	0.010	0.001
N4139	Bal	8.7	0.82	0.21	0.003	0.009	0.001

Table 4.2.6 Examples of gating system dimensions and coating thickness

Melt No.	Dimensions (mm)				Pattern density (g/cm ³)	Coating thickness (mm)
	Sprue	Runner	Ingate	Riser		
Top Gating System						
N4080	18 x 18	18 x 18	9 x 18	24 x 24	0.021	0.2
N4086	18 x 18	24 x 24	9 x 18	24 x 24	0.021	0.2
N4086	24 x 24	24 x 24	9 x 18	None	0.021	0.2
N4087	18 x 18	18 x 18	9 x 18	24 x 24	0.026	0.2
N4087	18 x 18	24 x 24	9 x 18	24 x 24	0.026	0.2
Side Gating System						
N4121	18 x 18	No runner	12 x 24	24 x 24	0.021	0.2
N4125	18 x 18	No runner	12 x 24	24 x 24	0.026	0.2
N4127	24 x 24	No runner	12 x 24	24 x 24	0.021	0.2
N4127	24 x 24	No runner	12 x 24	24 x 24	0.026	0.2

4.2.2.1 Application of Vacuum

Castings poured under vacuum application for top- and side-gating designs are shown Figures 4.2.3 and 4.2.4. The castings are filled and free from visual casting defects. However, castings poured without the application of vacuum during pouring and solidification not filled. Figure 4.2.5 shows an example of castings poured at 730°C without vacuum application. The casting was not filled showing misrun, shrinkage, and surface porosity. The lack of filling is associated with the build-up of backpressure in the gating system during pouring and solidification. The improved mold filling with vacuum application demonstrates the beneficial effect of vacuum as it helps to extract the mold gases during the degradation of the foam pattern.

Table 4.2.7 Examples of processing temperatures and casting weight

Melt No.	Pouring		Pattern density (g/cm ³)	Gating Ratio(1)	Casting weight (g)		Casting yield (%)
	Temp. (°C)	Time(s)			Total	Casting	
Top Gating System							
N4080	730	3	0.024	1:1:1	985	790	80
N4086	730	4	0.024	1:1.8:1	1040	790	76
N4086	730	4.5	0.024	1.8:1.8:1	1105	790	71
N4087	730	3	0.026	1:1:1	1055	860	82
N4087	730	4	0.026	1:1.8:1	1110	860	77
Side Gating System							
N4121	730	3	0.024	0.6:1	965	790	82
N4125	730	3	0.026	0.6:1	1035	860	83
N4127	730	4	0.024	1:1	1025	790	77
N4127	730	4	0.026	1:1	1095	860	79

¹Gating ratio defined as: sprue base or choke area: runner area: ingate area.

4.2.2.2 Gating System Design and Foam Density

The following general comments could be made about the top- and side-gating system designs. Figures 4.2.3 (a) and (b) show the two sides of the same casting. The casting was free from surface defects. For the top-gating system design, shown in Figures 4.2.3 (a) and (b) it was shown that castings from the lower density foam, 0.024 g/cm³ (1.3 lb/ft³) pattern tended to be defect free. The same observation was made for the side-gated castings shown in Figures 4.2.4 (a) and (b). The quality of the castings produced with the 1:1:1 gating ratio is similar to that from 1:1.8:1, and the respective casting yields were 80 and 76%, respectively (Table 4.2.7). In this particular case, there was no benefit in increasing the runner dimensions. The castings from the higher-density foam, 0.026 g/cm³ (1.6 lb/ft³) tended to show surface shrinkage and gas defects.

The above observations seem to suggest that a lower-density EPS foam pattern is preferable over higher density patterns for Mg alloy AZ91E as defects are reduced or eliminated. The gating system design is not as important as the foam density in terms of defect generation. The reduced defects encountered from a lower-density foam pattern could be attributed to a decrease in the decomposition products ahead of the solidification front during the degradation of the foam pattern. This result seems to suggest that the significance of gating ratios for open-cavity molds is not the same as that required for lost-foam casting. In an open-cavity mold, for a constant volume flow rate of liquid, the velocity of the stream is inversely proportional to the cross-sectional area of the channel in which it is flowing. It is desirable to have the metal enter the casting cavity at minimum velocity and hence with minimum turbulence. For this to happen, the cross-sectional area of the ingates is set equal to or greater than that of the runner so that the liquid metal moves at a decreasing velocity through successive channels of the increasing cross-sectional area (an “un-pressurized” gating system).

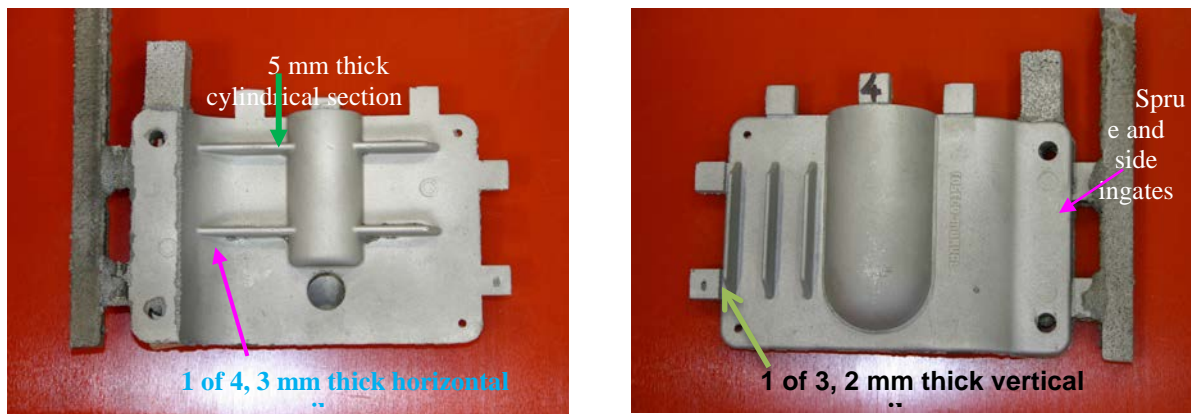
In lost-foam casting, the solid sprue, runner, and ingate have to be vaporized during pouring. Hence, the larger the gating system dimensions, the more foam decomposition products that need to be vaporized before casting solidification are generated ahead of the solidification front. The traditional gating ratio cannot be applied to lost-foam casting. This observation is similar to that reported by previous investigators for aluminum alloys during the casting of 4.8 mm (0.188 in.) thick lost-foam plates⁸⁻¹¹.

They reported that the size of the gating system had little effect on mold filling and metal velocity in lost foam casting process. However, lower foam density and higher coating permeability resulted in higher fill velocity. They noted that the significance of the sprue, runner, and ingate design is related to the control and removal of foam decomposition products during mold filling.

It is anticipated that the use of a hollow sprue and possibly runner instead of solid sprue and runner should further improve mold filling, reduce the volume of pyrolysis products, and lead to improved casting quality. It is noted that hollow sprue or runner systems were not used in this experiment. The top gating design leads to a steady flow of liquid and also creates more favourable conditions for directional solidification of casting from the bottom towards the casting ingate and runner systems. The side gating did not require a runner as the ingates were glued directly to the sprue resulting in improved casting yield.

4.2.2.3 Molding Media

The molding media used in this study were silica sand with 50 GFN and CarboAccucast-ID40™ – a synthetic mullite with 39 GFN. Based on the results of a comparison of the four melts from the CarboAccucast-ID40™ with the ten melts from the silica sand, the following observations were made. In general, good castings could be produced from the two molding media when vacuum was applied. This shows that the two molding media show adequate permeability with the vacuum application. Full castings could not be produced from either molding media when vacuum was not applied.



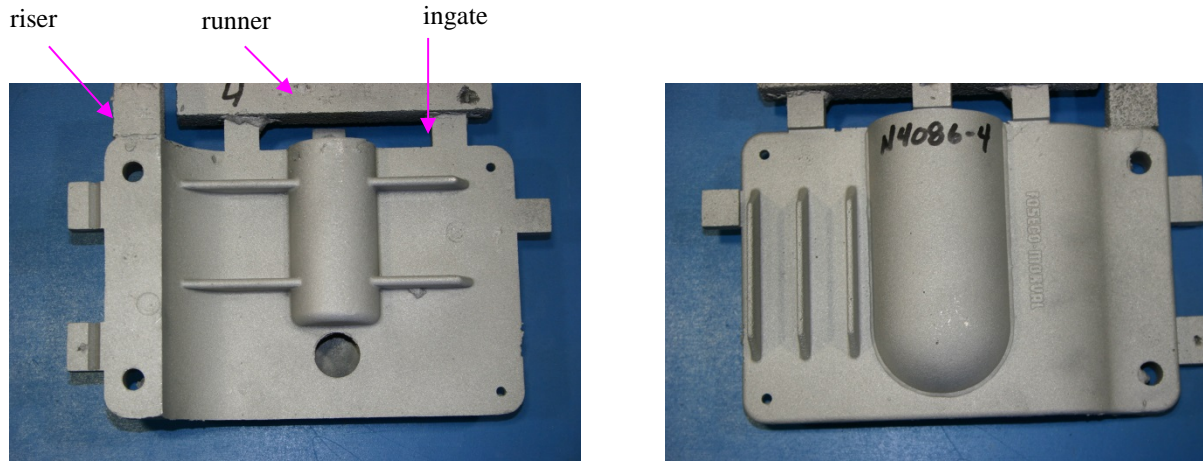
(a) N4121-0393, front of casting.

(b) N4121-0392, back of casting.

Figure 4.2.3 Defect-free castings from side-gated castings poured at 730°C. Vacuum was applied during pouring. Alloy AZ91E.

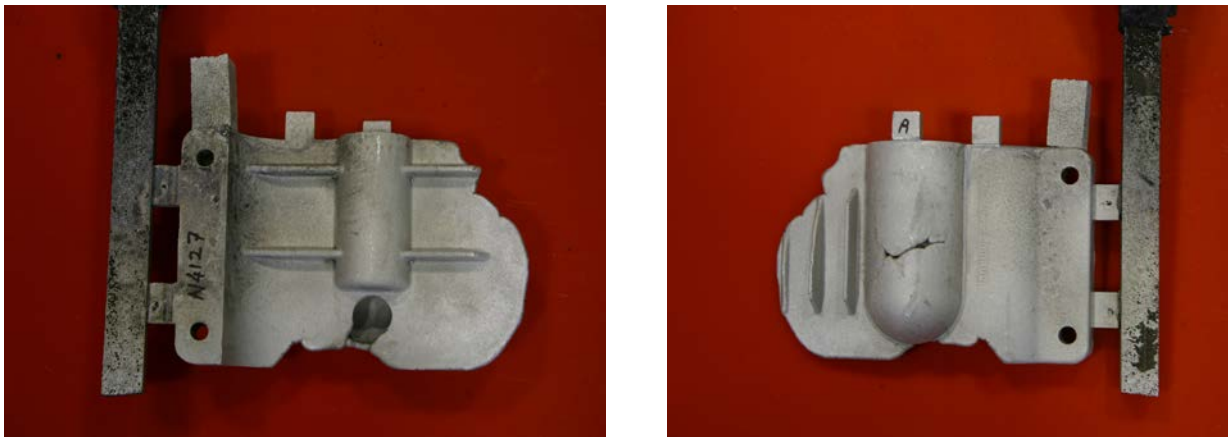
It is noted that the liquidus and solidus temperatures of AZ91E were 598°C (1108°F) and 468°C (874°F) giving a long solidification range of 130°C for this alloy. The pouring temperatures measured by an immersed thermocouple ranged from 700-780°C (1292-1436°F), with a superheat of 102-182°C (216-260°F). Mold filling improved at higher pouring temperatures. The effect of pouring temperature was evaluated for the top gating system with gating ratio 1.8:1.8:1 by pouring castings at 720, 740, and 780°C (1328, 1364, and 1436°F). Visual examination of the castings poured show that higher metal superheat improved the surface finish and resulted in the elimination of misrun. Higher metal superheat leads to the vaporization of the foam degradation products and reduced possibility of entrapping liquid polymer in the solidifying casting. Low metal superheat could lead to the transportation and subsequent entrapment of liquid polystyrene into the solidifying metal, leading to the formation of porosity and fold defects. The

maximum pouring temperature used in this study was 780°C (1436°F); this was found to be sufficient to vaporize any polystyrene decomposition products.



(a) N4086-0230, front of casting. (b) N4086-0229, back of casting in (a).

Figure 4.2.4 Defect-free castings from top-gated castings poured at 730°C. Vacuum was applied during pouring. Alloy AZ91E.



(a) N4127-0379, front of casting. (b) N4127-0378, same as (a), back of casting.

Figure 4.2.5 Castings poured at 730°C without vacuum application. Full castings could not be produced. Alloy AZ91E.

4.2.2.4 Metallography and X-Ray Analyses

Three test samples were sectioned from the 5 mm and 25 mm thick sections of well-filled castings for metallographic examination. The samples were cold mounted using epoxy resin, polished, and etched using a Glycol (1 mL HNO₃, 75 mL ethylene glycol and 25 mL distilled H₂O). Optical photographs of the microstructures were obtained at low and high magnifications. Three castings were X-rayed to evaluate the casting soundness. A photograph of a foam casting and the cross-section from where samples were obtained is shown in Figure 4.2.6. Examples of microstructures from the 25 mm and 5 mm thick sections of the widget foam casting are shown in Figure 4.2.7. The thicker sections show some

shrinkage porosity (Figure 4.2.7a) that tended to occur in the last region to solidify. This microstructure is consistent with those from alloys with a relatively long solidification range (130°C). The 5 mm section was relatively free of shrinkage porosity (Figure 4.2.7c). The microstructures from sections C and B are similar as both sections are 5 mm in thickness. At higher magnifications, the 25 mm and 5 mm sections are shown in Figures 4.2.7 (b) and (d), respectively. The microstructures show some massive $Mg_{17}Al_{12}$ inter-metallic compound, containing globules of magnesium solid solution, surrounded by lamellar $Mg_{17}Al_{12}$ that precipitated during solidification, similar to that shown in the ASM Handbook²². The relatively slow cooling rate during the lost-foam casting process resulted in this segregated type of eutectic structure.

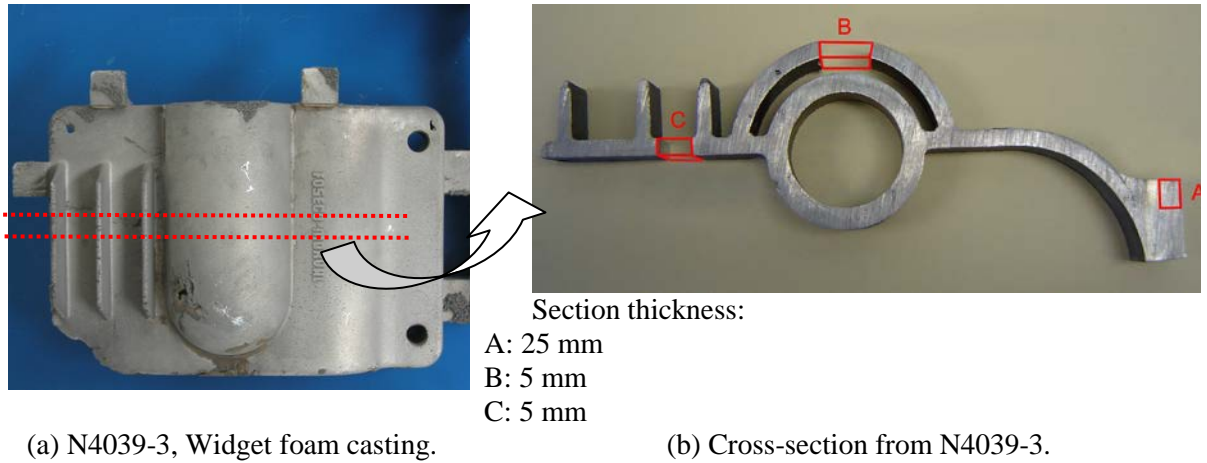
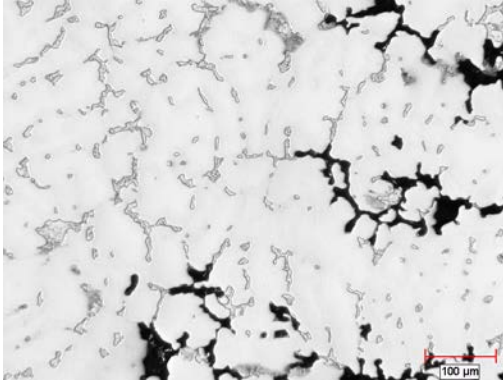
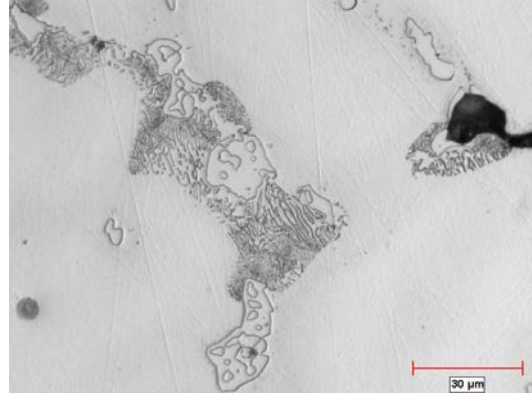


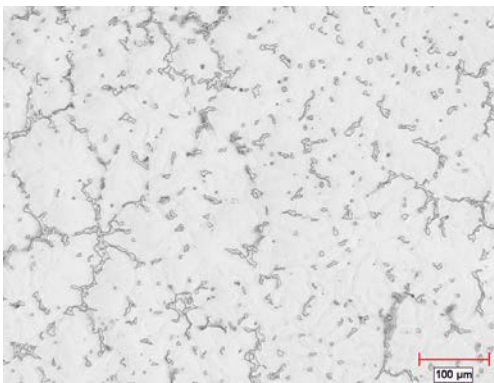
Figure 4.2.6 Widget casting showing where samples were removed for metallography.



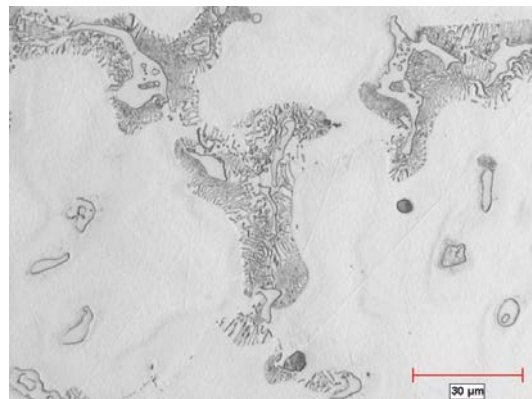
(a) N4039-3A, 25 mm thick -img01-100x.



(b) N4039-3A img02-500x.



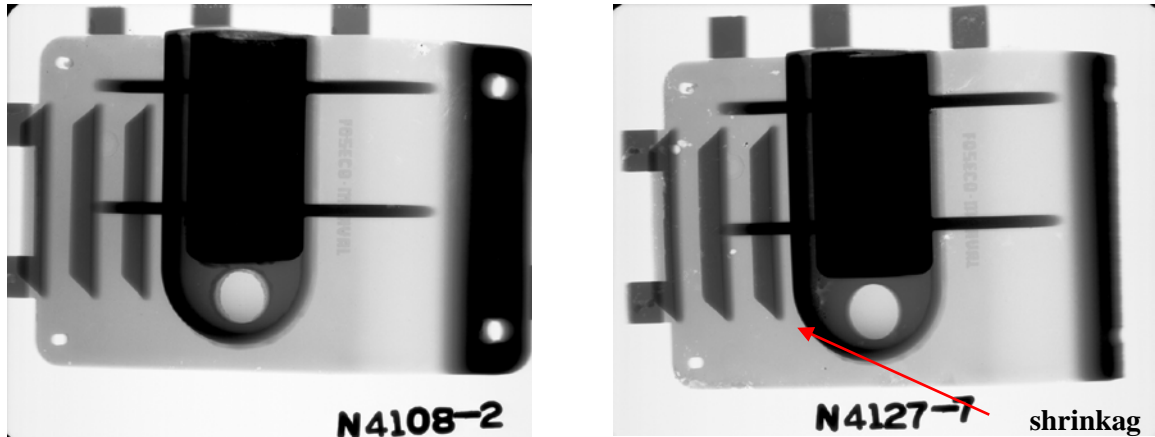
(c) N4039-3B, 5 mm thick -img01-100x.



(d) N4039-3B, 5 mm thick -img02-500x.

Figure 4.2.7 Microstructures from 25 mm and 5 mm thick sections. Glycol Etch.

Examples of X-ray radiography from selected castings produced using vacuum are shown in Figure 4.2.8 (a) and (b). The X-ray analysis was only qualitative, and no comparison was made with the ASTM standards. Nevertheless, the following observations could be made. The casting shown in Figure 4.2.8 (a) is relatively free of internal shrinkage defects. Internal shrinkage and inclusion defects are present in thicker sections of the casting, especially in areas close to change of dimensions or hot spots where the two pattern segments were glued together as shown in Figure 4.2.8(b).



(a) N4108-2a

(b) N4127-7a, some shrinkage defect.

Figure 4.2.8 X-ray radiography from selected castings using vacuum.

4.2.2.5 Summary and Conclusions

1. The castings poured without the application of vacuum were not filled, even at the maximum pouring temperature used in this investigation (780°C with a 182°C superheat). The non-filling can be associated with the build-up of backpressure in the gating system during pouring and solidification.
2. The application of -70 to -80 kPa (-10.15 to -11.6 psi) vacuum was adequate to facilitate the complete filling of the foam patterns poured at 730°C with a 132°C superheat – even the 2 mm thick vertical ribs in the foam patterns were filled completely.
3. Reduced casting defects (e.g., misrun, rough surface, etc.) were observed when using lower density foam pattern and higher pouring temperature (higher metal superheat).
4. Both side and top gating system designs can be used for magnesium alloy AZ91E.
5. The traditional gating ratio concept does not seem to apply for lost-foam gating system design. There was no significant improvement in mold filling at higher gating ratios.

4.2.3 Castings Poured from AZ91D and AM50

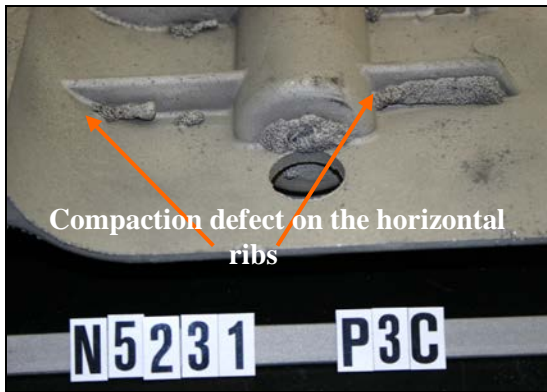
The chemical analysis from three melts is shown in Table 4.2.8. The composition generally falls within the levels recommended for this alloy²¹. Figure 4.2.2 is a photograph of a typical widget casting cluster (regular EPS foam pattern glued to the hollow fiber sprue and poured at 725°C). It is apparent that the levels of filling for each of the widget patterns are different. The difference in the level of filling is associated with the type of coating used for each foam pattern in the cluster.

The types of casting defects observed in alloy AZ91D are shown in Figure 4.2.9. The liquidus and solidus temperatures of this alloy are 598°C (1108°F) and 468°C (874°F), respectively, giving a long solidification range of 130°C (234°F). The common defects observed are compaction defects, Figure 4.2.9 (a); folds and misruns defects, Figures 4.2.9 (b) and (c); and gas tracks defects, Figure 4.2.9(d). The compaction defects were present mainly along the horizontal fins of the widgets that were difficult to fill with molding sand during vibration.

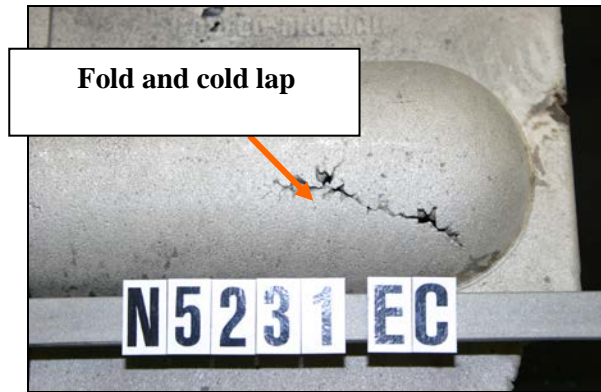
Due to the relatively weak glue joint between the foam pattern and the hollow fiber pouring sprue, minimal vibration was applied during compaction. In future casting trials, with stronger glue joints and increased vibration, this type of defect can be eliminated. The misrun/cold lap and fold defects were more common in castings poured at 725°C (127°C superheat) and less common for those poured at 775°C (177°C superheat). These observations were expected, as the pouring temperature influences the casting fluidity, the rate of decomposition of the pattern, the nature of the pyrolysis products, and the rate of removal during casting solidification. Given the lower heat content of magnesium compared with aluminum, this result seems to suggest that higher metal superheat would be required for magnesium alloys to reduce misrun and other solidification-related casting defects.

Table 4.2.8 Chemical analyses of magnesium alloys AZ91D and AM50

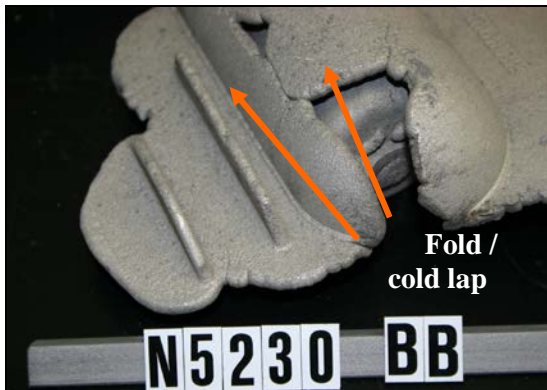
Melt No.	Composition (wt %)						
	Mg	Al	Zn	Mn	Fe	Cu	Ni
ASM spec. AZ91D	Bal	8.1-9.3	0.4-1.0	0.17-0.35	0.005 max	0.015 max	0.0010 max
N5230	Bal	8.0	0.45	0.19	0.001	<0.001	0.001
N5231	Bal	8.3	0.45	0.18	<0.002	<0.005	0.001
ASM spec. AM50	Bal	4.4-5.4	0.22 max	0.26-0.60	0.004 max	0.010 max	0.002 max
N5181	Bal	5.0	0.02	0.31	0.001	0.001	0.001



(a) N5231-P3C, compaction.



(b) N5231-EC, fold and cold lap.



(c) N5230-BB, misrun, fold and cold lap.



(d) N5231-EC, gas tracks.

Figure 4.2.9 Examples of casting defects on widget castings poured from Mg alloy AZ91D.

4.2.3.1 Widget Castings Poured from AZ91D Using Hollow Sprue

Thirty-two widget castings were poured, half at 725°C and the other half at 775°C for four different foam and coating types. The average weight of each full widget poured at 775°C was about 0.865 kg, and the weight of the solidified hollow sprue was 5.2 kg. Photographs of each of the widget castings are shown in Figure 4.2.10. The castings are arranged according to foam and coating type and pouring temperature. Each of the four castings in rows A, B, C and D are coated with the same coating and listed according to the coating reference in Table 4.2.3. The four castings in columns P3, E, P7, and B were poured in the same type of foam and are listed by foam reference in Table 4. 2.1. None of the widget patterns poured at 725°C (127°C superheat) were filled, Figure 4.2.10a. The worst castings were produced from the Brominated EPS pattern (B) (last column), and the best from Probead 70 (P7) foams (third column). It is noted that there was a breakout during the pouring of the Brominated EPS pattern which halted filling. For the castings poured at 775°C, patterns coated with the Styromol 169.23 (A) coating resulted in the best filling with good surface finish bottom row, Figure 4.2.10b. The three, 2 mm vertical fins in each pattern were filled, but two of the widgets did not quite fill at the bottom furthest from the ingate. The improvement in mold filling and surface finish is probably associated with the fact that mica is more neutral to magnesium than the silica or alumino silicate that were the major ingredients in the other coatings. In addition, the coating also has high insulating properties that reduced heat loss in the molten metal during mold filling. Both Sempocperm M66L (B) and Sempocperm 70 (C) coatings produced good surface finish for AZ91D. Patterns coated with Styromol 140.31 (D) had the most missing sections (Row 1). It is noted that Styromol 140.31 is silica based and possibly reacted with the molten magnesium during mold filling, Table 4.2.3. These results seem to suggest that a combination of high pouring temperature and Styromol 169.23 coating produced good castings AZ91D.



(a) N5230, AZ91D Castings poured at 725°C (127°C superheat).



(b) N5231, AZ91D Castings poured at 775°C (177°C superheat).

Figure 4.2.10 Widget castings poured at (a) 725°C and (b) 775°C. The extent of mold filling, casting defects, and surface quality are shown for each of the casting.

4.2.3.2 Plate, Box, and Widget Castings Poured from AM50

All of the plate, box, and widget prototype castings poured from AM50 were poured using a solid EPS sprue. The processing parameters for the plate, box, and widget pattern are given in Tables 4.2.9, 4.2.10 and 4.2.11, respectively. In general, castings poured without application of vacuum did not fill completely. The common surface defects were poor compaction, misrun, and poor surface finish in a number of castings. The lack of filling could be associated with the build-up of backpressure in the gating system during pouring and solidification. The application of vacuum during pouring improved the extraction of the mold gases generated during the degradation of the foam pattern. Pouring the castings at higher temperatures improved mold filling and surface finish as the higher metal superheat speeds up the vaporization of the foam degradation products. Low metal superheat could cause liquid polystyrene to move into the solidifying metal and become trapped, leading to the formation of porosity and fold defects.

Table 4.2.9 Gravity and vacuum assisted pouring of the plate patterns

Cast No.	Plate thickness (mm)	Sprue* height (cm)	Applied vacuum (kPa)**	Pouring Temp. (°C)	Comments
6	12	400	0	760	Almost filled
10	12	400	-40	720	Filled
11	24	400	-40	720	Filled
15	24	400	0	720	Not filled

*Sprue EPS foam density: 0.0240 g/cm³ (1.5 lb/ft³); 2.54 cm x 3.18 cm, 2 side ingates.

**Applied vacuum: -41 kPa (-6 psi).

Table 4.2.10 Gravity and vacuum assisted pouring of the box pattern

Cast No.	Sprue* height (cm)	Applied Vacuum (kPa)**	Pouring Temp. (°C)	Comments
3	40.6	0	760	Filled, compaction defect
4	40.6	-40	760	Filled, compaction defect

*Sprue EPS foam density: 0.0240 g/cm³ (1.5 lb/ft³); 2.54 cm x 3.18 cm, 2 side ingates.

**Applied vacuum: -41 kPa (-6 psi).

It is noted that the liquidus temperature of AM50 is 620°C. The foam pattern castings were poured at 720°C and 760°C giving melt superheats of 100°C and 140°C, respectively. Table 4.2.9 shows that the 12 mm plate casting poured at 760°C and the 12 and 24 mm plate castings poured at 720°C without vacuum assistance did not fill. With vacuum assistance, the 12 and 24 mm plate castings poured at 720°C filled. The applied vacuum during the casting trials was -40 kPa (-6 psi). Photographs of the plate and box patterns, as well as the widget pattern are shown in Figures 4.2.11, 4.2.12, and 4.2.13, respectively. The photographs of the 24 mm plate castings poured without and with vacuum assistance are shown in Figures 4.2.11(a) and (b), respectively. The plate, Figure 4.2.11(a) and box pattern castings poured at 720°C without vacuum assistance did not fill. The box patterns poured at 760°C with and without vacuum application filled. Photographs of the front and back of a filled box casting are shown in Figure 4.2.12 (a) and (b). The complexity of the box casting might have contributed to the inconsistent filling, and a compaction defect is readily apparent inside the box casting (Figure 4.2.12b). Photographs of the widget castings poured at 760°C without and with vacuum assistance are shown in Figures 4.2.13(a) and

(b), respectively. The widget casting was not filled, even when poured at 760°C - the highest pouring temperature used during the casting trial. This seems to suggest that, because of its relative complexity and thin wall sections, pouring temperatures in excess of 760°C would be required to fill this pattern when using solid EPS sprues.

Table 4.2.11 Gravity and vacuum assisted pouring of the widget pattern

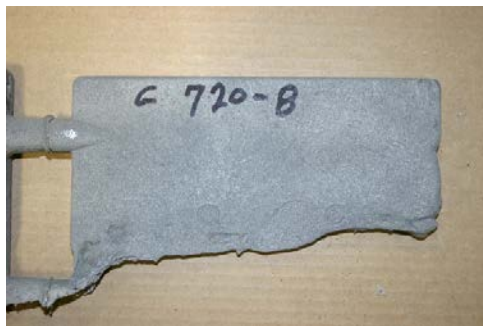
CastNo.	Sprue Height (cm)*	Applied Vacuum (kPa)**	Pouring Temp. (°C)	Comments
1	28	-40	760	Filled
5	28	0	760	Not Filled
7	28	0	720	Not filled
13	28	-40	720	Filled

*Foam density: 0.0256 g/cm³ (1.6 lb/ft³); EPS foam pattern, 1.9 cm x 1.9 cm, 2 side ingates.

** Applied vacuum: -40 kPa (-6 psi).

4.2.3.3 Analysis of Fold Defects in Box and Widget Castings

In order to detect fold and inclusion defects, some castings were broken and the fractured surface examined. Fold defects were readily apparent on the surfaces of the fractured samples from the box and widget castings in alloy AM50, Figure 4.2.14(a) and (b). These defects could be due to the geometries of the box and widget castings where abrupt changes in section thickness and sharp corners promoted turbulent mold filling and entrapment of foam degradation products during solidification. These castings were poured at 720°C (100°C superheat). Given the low heat content of magnesium alloys, higher pouring temperature and improvements in casting design (avoiding sudden section thickness changes) should eliminate these types of defects. Limited analysis of the oxide and fold defects was performed by SEM examination of the fracture surface of the widget casting shown in Figure 4.2.14(b). The clean area is shown in Figure 4.2.15(a), and Figure 4.2.15(b) and (c) show the area with the foam residue/oxide film. Figure 4.2.15(c) shows the SEM EDS analysis of the area in Figure 4.2.15(b). Strong peaks of magnesium, aluminum, oxygen and carbon are observed, suggesting that the defect observed is a combination of foam degradation products and spinel. Figure 4.2.15(d) shows the dendritic nature of the alloy and porosity.



(a) N5181-8c, no vacuum.



(b) N5181-10c, vacuum, -40 kPa. (-6 psi).

Figure 4.2.11 24 mm plate casting poured at 720°C from AM50.



(a) N5181-3c, back.



Compaction defect

(b) N5181-3c, front.

Figure 4.2.12 Box casting, poured at 760°C from AM50 without vacuum assistance.



(a) N5181-5c, no vacuum, not filled, misrun.

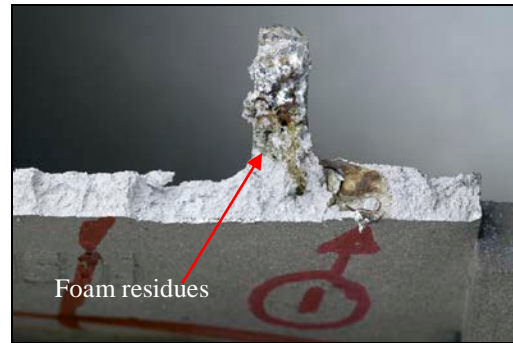


(b) N5181-1c, vacuum, (-40kPa), filled.

Figure 4.2.13 Widget castings poured at 760°C from AM50.

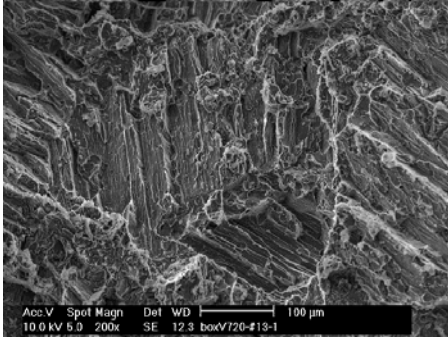


(a) N5181-12-4, Box casting.

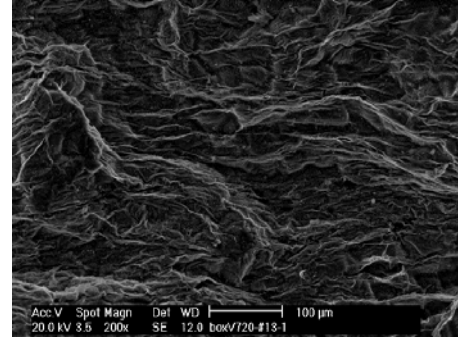


(b) N5181-13-1, Widget casting.

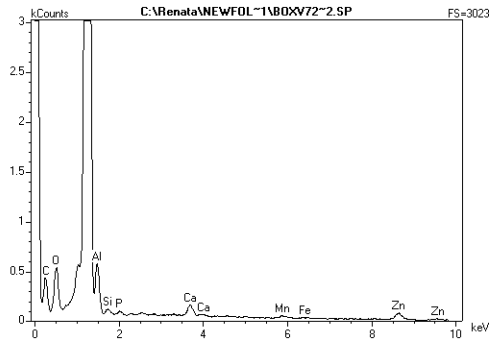
Figure 4.2.14 Fracture surfaces from box casting poured at 720°C showing fold defects.



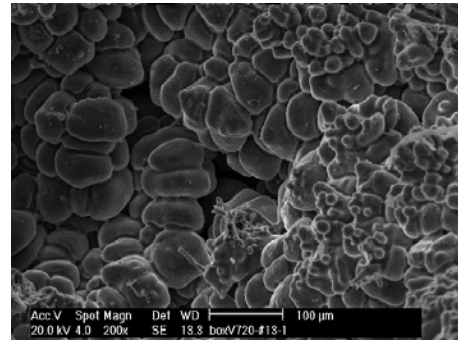
(a) N5181-13-1, oxide free, 200x.



(b) N5181-13-1, oxide layer, 200x.



(c) N5181-13-1, EDS analysis of (b).

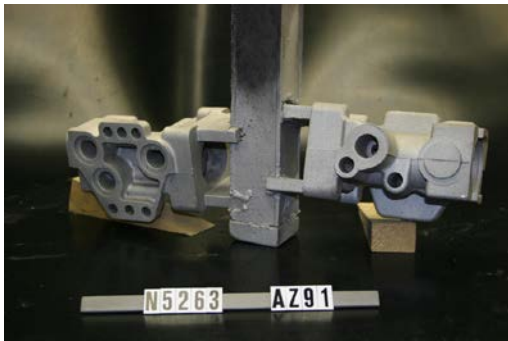


(d) N5181-13-1, porosity and dendritic structure.

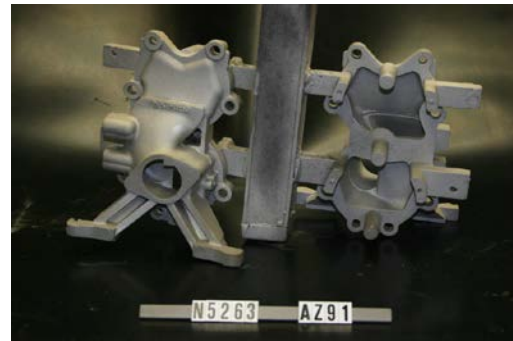
Figure 4.2.15 SEM of fracture surface from the widget pattern casting showing (a) clean area, and fold defects: (b) oxide film, (c) EDS of (b) and (d) dendritic structure and porosity.

4.2.3.4 Elx-Body and Intake-Manifold Castings Poured from AZ91D

The prototype castings were poured using a hollow EPS sprue. Photographs of the Elx-body and Intake manifold castings poured from AZ91D are shown in Figure 4.2.16 (a) and (b), respectively. It is noted that these components were poured using the hollow EPS sprue and the Carboceramic backing sand without vacuum assistance. It is apparent that both components show good surface finish without any misrun as they were poured with adequate melt superheat. A compaction defect can be observed in the Elx-body casting, Figure 4.2.17(a). This is associated with poor compaction during pattern vibration. This is one of the major defects observed in this pattern because of its rather complex casting geometry. The intake manifold was free of surface defects. These two castings have demonstrated the potential of magnesium lost foam-casting for production parts.

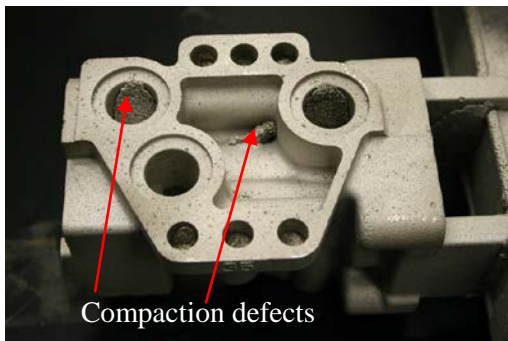


(a) Elx-body casting.



(b) Intake-manifold.

Figure 4.2.16 Elx-body and intake-manifold foam casting assembly.



(a) Side 1, Elx-body casting, compaction defect.



(b) Side 2, Elx-body casting, good surface finish.

Figure 4.2.17 Elx-body showing compaction defect and good surface finish.

4.2.3.5 Summary and Conclusions

Currently, there is no commercial foundry in North America dedicated to lost foam casting of magnesium alloys; CANMET-MTL is one of few R&D laboratories in North America with a focused research program on this technology. The beneficial effect of vacuum application during lost foam casting of prototype components of selected magnesium alloys has been demonstrated. We have also tried new foam patterns based on new polymer bead materials and new coating formulations that have the potential of producing good quality castings from magnesium alloys. The following conclusions are made:

1. The casting trials demonstrated that engineering components could be cast successfully in magnesium alloys AZ91D and AM50 by the lost foam casting process.
2. Four foam types (Brominated EPS, regular EPS, Probead 30 and Probead 70) were tested. Based on the degree of filling, misruns, and surface finish, the best castings were produced using the Probead 70 foam pattern, and the worst from the Brominated EPS pattern. The poor result from the Brominated EPS pattern may be associated with the breakout that occurred during pouring at a lower temperature. Further study is required to gain a better understanding.
3. Four coatings (Styromol 140.31, Styromol 169.23, Sencoperm M66L, and Sencoperm M70) were applied to each of the foams and tested at two pouring temperatures. Styromol 169.23 produced the most complete castings with good surface finish and the sharpest features. These results seem to suggest that the use of high pouring temperature and Styromol 169.23 coating is a good combination for Mg alloy AZ91D.
4. Both Sencoperm M70 and Sencoperm M66L coatings may be used for Mg alloy AZ91D.
5. The application of -40 kPa (-6 psi) vacuum facilitated the complete filling of the widget, box, and plate patterns in alloy AM50 with 100°C or 140°C superheat.
6. Fold defects similar to those found in aluminum alloys can be expected in cast magnesium alloys, especially with patterns of complex geometry, such as the box and widget patterns. These promote turbulent mold filling that lead to the entrapment of foam degradation products during solidification.
7. Given the low heat content of magnesium alloys, higher pouring temperatures and improvements in the casting and gating design are necessary to ensure complete mold filling, and eliminate fold and misrun defects.
8. The use of hollow sprue improved the filling of the widget patterns.
9. The role of coating permeability on casting quality is not clear at this time. The Styromol 169.23 coating with lower permeability than the Sencoperm coatings produced the best castings. Given that Styromol 169.23 coating is mica based and the Sencoperm coatings are alumino-silicate based, the effect of the coating refractory base is perhaps as important as its permeability.

4.3 TASK 3 Mechanical Properties and Metallography

The key focus is the evaluation of the mechanical properties (UTS, YS, and % elongation) of magnesium alloys AZ91D, AM50 and ZE41 determined from lost foam plate castings. The microstructures of sectioned test samples from plate castings were evaluated using optical metallography and scanning electron microscopy (SEM) techniques.

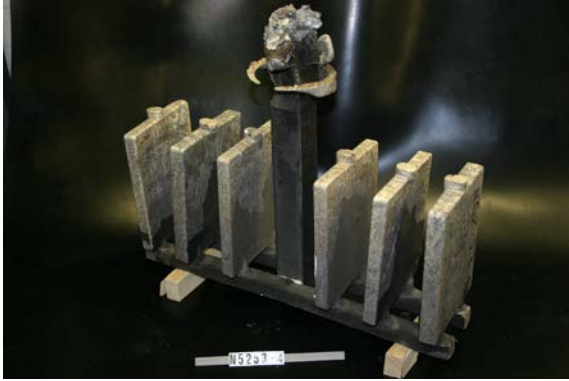
4.3.1 Experimental

The mechanical properties of magnesium alloys AZ91D, AM50 and ZE41 were determined from lost foam plate castings. The tensile properties of these three alloys were evaluated in both as-cast and heat-treated conditions. The microstructures and fracture surfaces were examined by optical microscopy and scanning electron microscopy (SEM) to evaluate the solidification structure and inclusion defects. The melting and pouring procedures were as described in Task 2. Specifically, the charge size for mechanical property evaluation of magnesium alloys AZ91D, AM50 and ZE41 ranged from 15-40 kg. The melting crucible was lifted to pour the plate castings at superheats ranging from 130-177°C. The nominal dimensions of the plate foam patterns were 203 mm (8 in.) long and 152 mm (6 in.) wide. The plate thicknesses evaluated were 12, 16, 20, and 24 mm (0.47, 0.63, 0.79 and 0.94 in.), and the density of the foam plate patterns was 0.0240 g/cm³ (1.5 lb/ft³).

The molding media used was a CarboAccucast-ID 40TM, a synthetic mullite with AFS 40 GFN. The thermophysical properties of the molding media are given in Table 4.2.4 This molding medium was selected for its low thermal expansion, high flowability, and high permeability. The patterns were coated with StyromolTM 169.23 - a mica-based standard foam coating for Al alloys with high insulating and permeability properties. The dipped patterns were hung to dry in air for 24-48 h before use. The estimated coating layer thickness after drying varied from 0.13 to 0.20 mm (0.005 to 0.008 in). The plate foam patterns were top or bottom gated through the premolded two-ingate section on the pattern. The sprues were partially hollow EPS 50.8 x 50.8 mm (2 x 2 in.), and the runners were 25.4 x 25.4 mm (1 x 1 in.). Photographs of both bottom and top gated plate castings are shown in Figures 4.3.1(a) and (b).

The plate castings were X-rayed, and test bars were machined from areas free of porosity or shrinkage defects. An X-ray of a 24 mm thick plate is shown in Figure 4.3.2. The machined round and rectangular test bars conform to ASTM B557M-02a and ASTM E 8M-04, respectively. The gauge length of the round bar was 62.5 mm, with 12.5 mm diameter. The gauge length of the rectangular bar was 50 mm with 12.5 mm width, and the overall length was 200 mm. The bar thicknesses were 8, 12, 16, 20 mm. Photographs of these test bars are shown in Figure 4.3.3.

The test bars were heat treated in a convection oven under argon atmosphere, and the samples were cooled to room temperature after solution treatment by fast fan cooling before aging. The heat-treatment process followed the procedures recommended in the ASM Specialty Handbook and is summarized in Table 4.3.1. It is noted that the round test bars were machined from the 24 mm thick plate castings. The mechanical properties were determined following standard ASTM procedures.



(a) Bottom gating



(b) Top gating

Figure 4.3.1 Photographs of plate foam clusters of (a) bottom and (b) top gated plate castings.

Samples for microstructural evaluation were sectioned from the gauge section of broken bars, then polished and etched. The fracture surfaces of selected samples were examined for the presence of oxide and other inclusions. The SEM image contrast from topographic and compositional differences were obtained using the low-energy secondary electrons (SE), the higher-energy backscattered electrons (BSE), and the energy-dispersive X-ray spectroscopy (EDS) to evaluate the solidification structure and the inclusion observed on the fracture surface of the test bars.

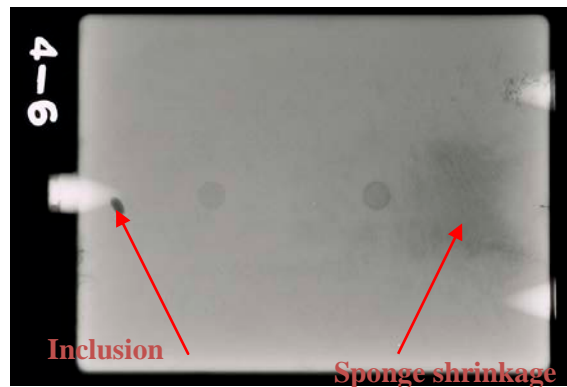
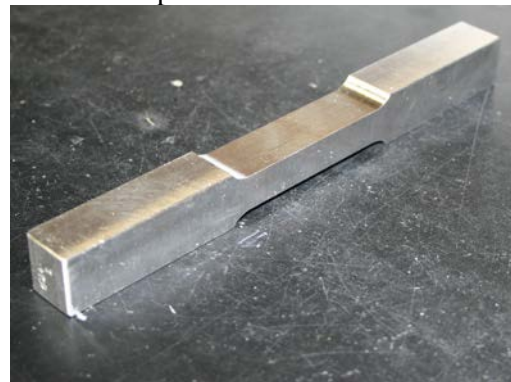


Figure 4.3.2 Sample X-ray of 24 mm thick plate.



(a) Round test bar.



(b) Rectangular bar.

Figure 4.3.3 Photographs of (a) round and (b) rectangular test bars.

Table 4.3.1 Heat treatment procedure for the test bars

Alloy/Temper	Heat Treatment Procedure
AZ91D-T6	Bars loaded at 260°C, and solutionized at 413°C for 16 h, followed by fast fan cooling. Samples were aged at 168°C for 16 h and air cooled.
AM50-T6	Bars loaded at 260°C, and solutionized at 424°C for 16 h, followed by fast fan cooling. Samples were aged at 232°C for 5 h and air cooled.
ZE41-T5	Bars solutionized at 329°C for 2 h and air cooled. Test bars were heat treated under argon atmosphere.

4.3.2 Results and Discussion

The chemical analysis from melts prepared and the ASTM specifications for the three alloys are shown in Table 4.3.2. The average mechanical properties, including the standard deviation (in bracket) and number of bars tested per sample type in the as-cast and after heat treatment for the three magnesium alloys are summarized in Tables 4.3.3 to 4.3.5. Some of the data in these tables are plotted in the graphs shown in Figures 4.3.4 and 4.3.5. The results in the tables show that acceptable mechanical properties can be achieved from the three alloys evaluated. Some improvement in tensile properties was observed after heat treatment. For the three magnesium alloys evaluated, mechanical properties can be improved by heat treatment as is the case with sand and permanent mold casting processes.

Table 4.3.2 Chemical composition range and analysis from melts prepared

Alloy	Melt No.	Composition, (Wt.%)						
		Al	Mn	Zn	Si	Cu	Zr	RE
AZ91D	ASTM	8.3-9.7	0.15-0.50	0.35-1.0	0.10	0.03	–	–
	N5263	7.5	0.18	0.38	0.008	–	–	–
AM50	ASTM	4.4-5.4	0.26-0.60	0.22 max	0.10	0.01	–	–
	N6014	4.54	0.29	<0.01	<0.01	<0.01	–	–
ZE41A	ASTM	-	0.15	3.5-5.0	–	0.10	0.40-1.0	0.75-1.75
	N5253	<0.010	0.012	3.90	<0.010	<0.005	0.278	0.767

Note: Rare Earth (RE) elements made up of 0.402%Ce, 0.312%La, and 0.053%Pr.

It is noted that there are currently no standard specifications for mechanical properties of lost foam cast magnesium alloys AZ91D, AM50, and ZE41A. Therefore, these results gives foundational insight into the type of mechanical properties that can be obtained from these alloys cast by lost foam casting process. There appears to be no strong correlation between the mechanical properties and the section thickness of the plate castings possibly due to the relatively slow cooling rate of the lost foam casting process. In addition, relatively high metal superheat was required to ensure complete filling of the plate castings cluster per melt. X-ray radiograph results show that shrinkage and oxide inclusion defects can be a problem. The observed defects can be reduced or eliminated by grain refinement and the use of steel mesh filters in the gating system. Summaries of the mechanical properties for each of the alloy are given below.

Table 4.3.3 Mechanical properties of AZ91D (Melt No. N5263)

Bar type/thickness (mm)	0.2% YS (MPa)	UTS (MPa)	Elong. (%)	No. of bars
As-cast				
Round	75 (4)	120 (10)	1.3 (0.3)	6
20	73 (1)	122 (6)	1.6 (0.2)	5
16	76 (3)	123 (10)	1.5 (0.4)	5
After T6				
Round	85 (3)	159 (17)	2.5 (0.8)	8
20	84 (1)	157 (12)	2.8 (0.7)	4
16	85 (5)	166 (24)	3.2 (1.8)	3

Table 4.3.4 Mechanical properties of AM50 (Melt No. N6014)

Bar type/thickness (mm)	0.2% YS (MPa)	UTS (MPa)	Elong. (%)	No. of bars
As-cast				
Round	54 (2)	123 (21)	3.8 (1.3)	5
20	60 (2)	158 (19)	5.9 (1.5)	3
16	62 (2)	165 (9)	6.5 (0.5)	3
12	63 (2)	151 (15)	5.2 (1.2)	4
After T6				
Round	60 (4)	133 (41)	3.8 (2.4)	5
20	64 (0.4)	185 (25)	8.3 (2.6)	4
16	64 (2)	178 (22)	7.5 (2.2)	4
12	65 (3)	149 (46)	5.9 (2.6)	4

Table 4.3.5 Mechanical properties of ZE41A (Melt No. N5253)

Bar type/ thickness (mm)	0.2% YS (MPa)	UTS (MPa)	Elong. (%)	No. of bars
As-cast				
Round	75 (6)	121 (10)	2.1 (0.7)	10
20	76 (6)	119 (8)	2.0 (0.8)	6
16	72 (2)	116 (5)	2.1 (0.4)	4
12	77 (7)	123 (7)	2.4 (0.4)	5
After T5				
Round	90 (2)	132 (4)	1.8 (0.3)	5
20	82 (2)	127 (5)	1.9 (0.5)	5
16	82 (0)	126 (4)	1.9 (0.2)	3
12	84 (5)	129 (12)	1.9 (0.8)	7

4.3.2.1 Alloy AZ91D, As Cast (F) and Heat Treated (T6)

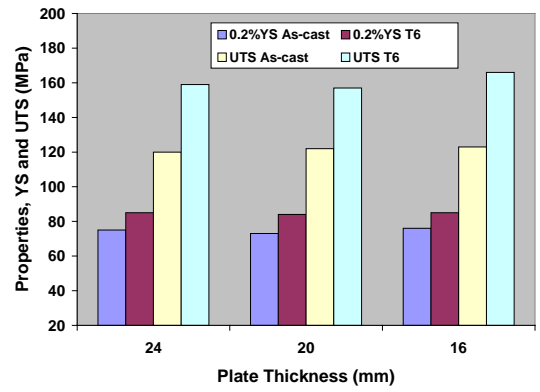
The YS, UTS, and elongation are comparable to those obtained from sand-cast test bars. The YS ranged from 73-76 MPa in the as-cast condition, and 84-85 MPa after heat treatment. The UTS ranged from 120-123 MPa as-cast, and 157-166 MPa after heat treatment. The % elongation ranged from 1.3-1.6% in the as-cast condition, and 2.5-3.2% after heat treatment. These results show that the tensile properties improve after heat treatment.

4.3.2.2 Alloy AM50, As Cast (F) and Heat Treated (T6)

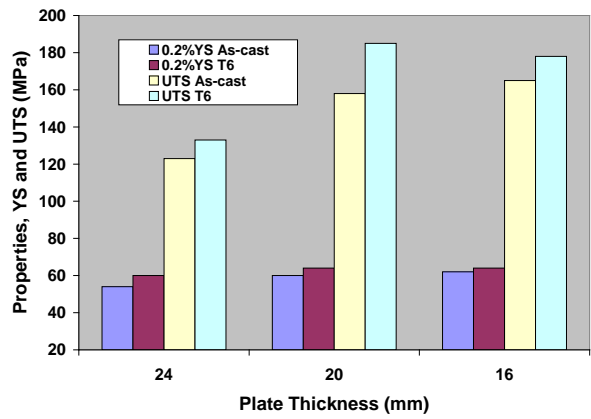
The YS ranged from 54-63 MPa in the as cast condition and 64-67 MPa after heat treatment. The UTS ranged from 121-165 MPa in the as-cast condition, and 133-185 MPa after heat treatment. The % elongation ranged from 3.8-6.5 % as-cast and 3.8-8.3% after T6 heat treatment. These results show modest improvement in tensile properties after heat treatment.

4.3.2.3 Alloy ZE41, As Cast (F) and Heat Treated (T5)

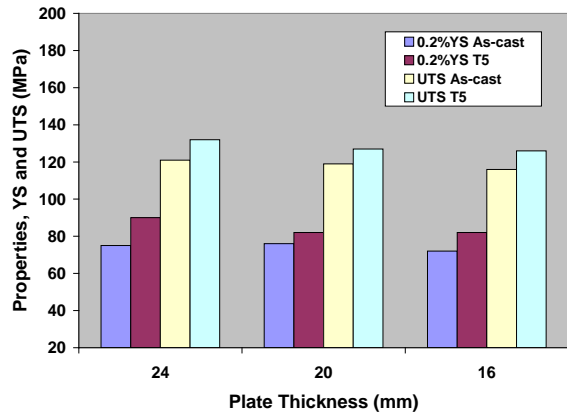
The YS ranged from 72-77 MPa as-cast, and 82-90 MPa after heat treatment. The UTS ranged from 116-123 MPa in the as-cast condition, and 126-132 MPa after heat treatment. The elongation ranged from 2.0-2.4% as cast and 1.8-1.9% after heat treatment. The tensile properties improved after heat treatment with a slight reduction in ductility.



(a) Alloy AZ91D.

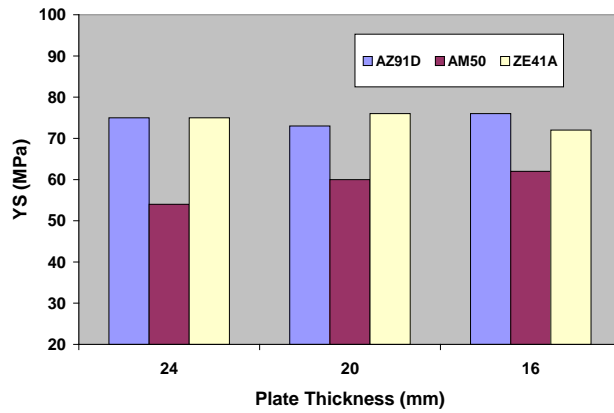


(b) Alloy AM50.

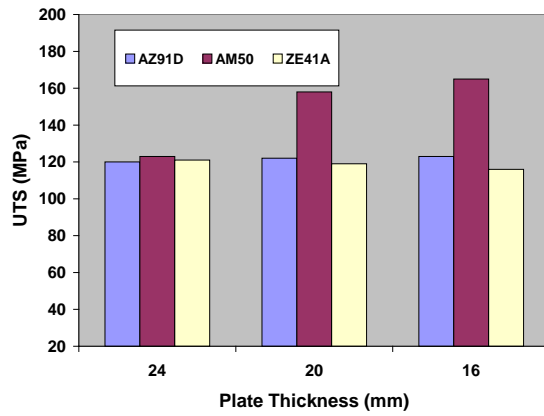


(c) Alloy ZE41A.

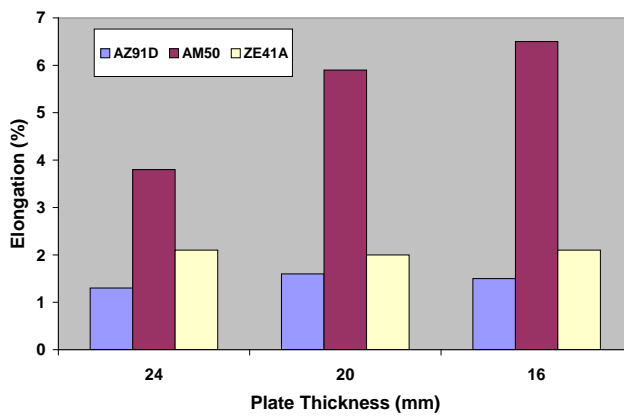
Figure 4.3.4 Tensile properties versus plate thickness for AZ91D, AM50 and ZE41A.



(a) Yield strength.



(b) Ultimate tensile strength.

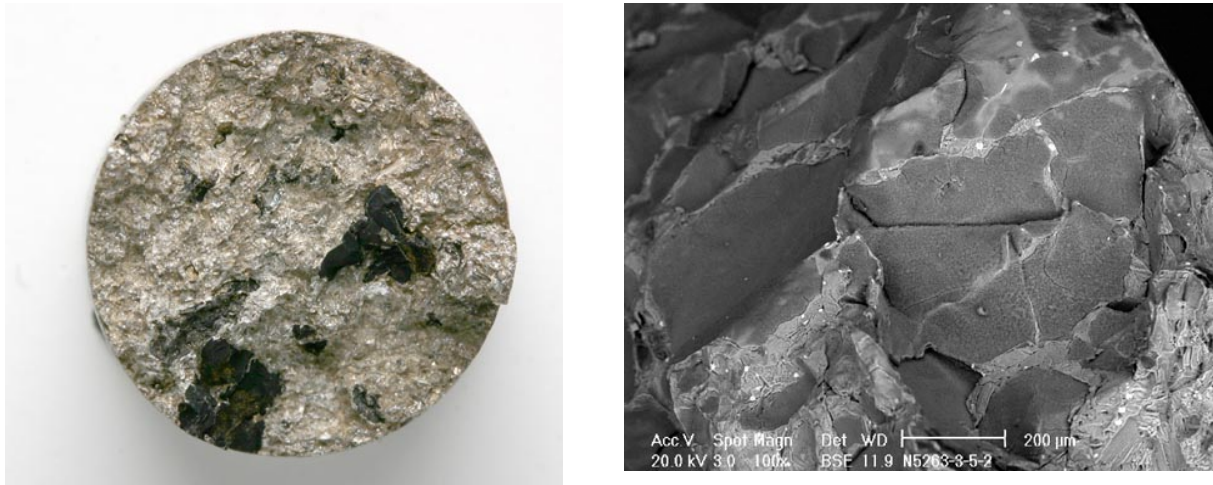


(c) Elongation.

Figure 4.3.5 Yield strength, ultimate tensile strength, and elongation in the as-cast condition.

4.3.2.4 Metallography and Microstructure

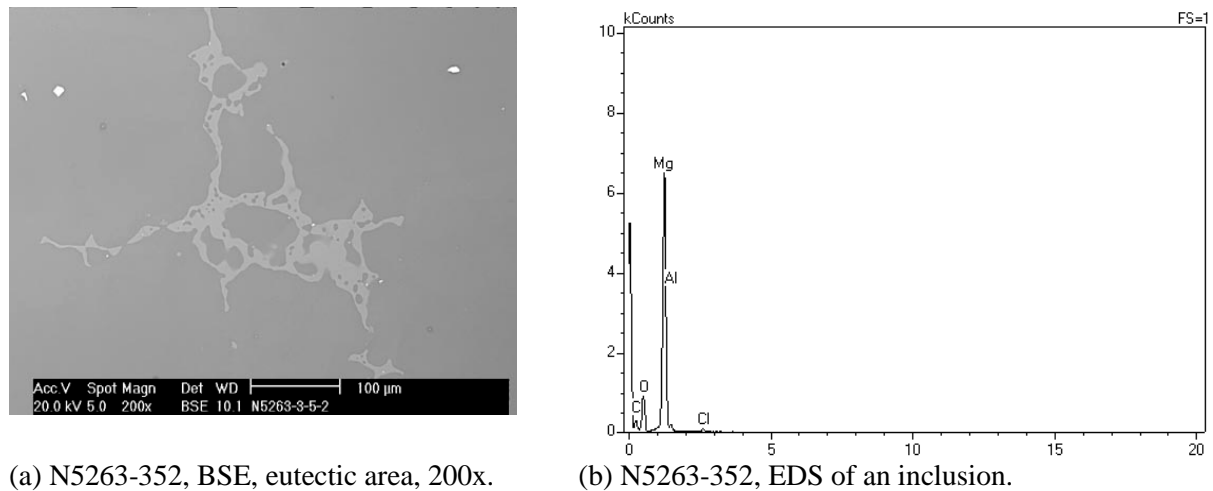
Examples of SEM images of the fracture surface from the AZ91D are shown Figure 4.3.6, and examples of SEM BSE of the eutectic area and EDS of an inclusion from AZ91D are shown Figure 4.3.7. The SEM BSE of the fracture surface from an as-cast broken test bar of alloy AM50 at low and high magnifications are shown in Figure 4.3.8(a) and (b), respectively. The dendritic structure of the alloy is readily apparent. Figure 4.3.9 shows the EDS spectra of the fracture surfaces shown in Figure 4.3.8(a) and (b) showing strong peaks of manganese, silicon, carbon, and oxygen.



(a) N5263-352, fracture surface, 5x.

(b) Same as (a) BSE, 100x,

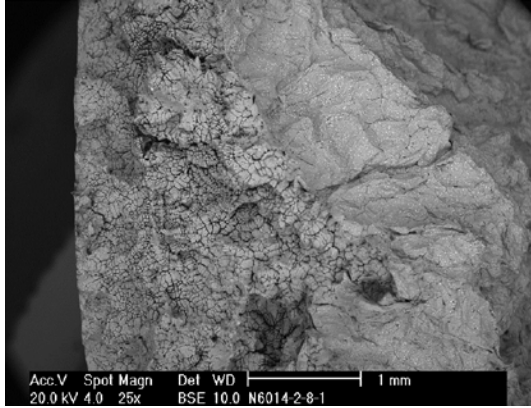
Figure 4.3.6 Microstructures from AZ91D round test bars machined from 24 mm thick plate.



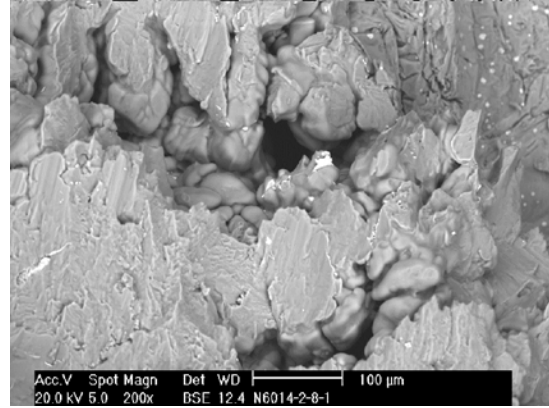
(a) N5263-352, BSE, eutectic area, 200x.

(b) N5263-352, EDS of an inclusion.

Figure 4.3.7 The BSE of (a) eutectic area and (b) EDS of an inclusion in AZ91D.



(a) AM50-N6014-281, BSE, fracture surface, 25x.



(b) AM50-N6014-281, BSE, fracture surface, 800x.

Figure 4.3.8 Fracture surface of a test bar from AM50 at (a) low and (b) higher magnifications.

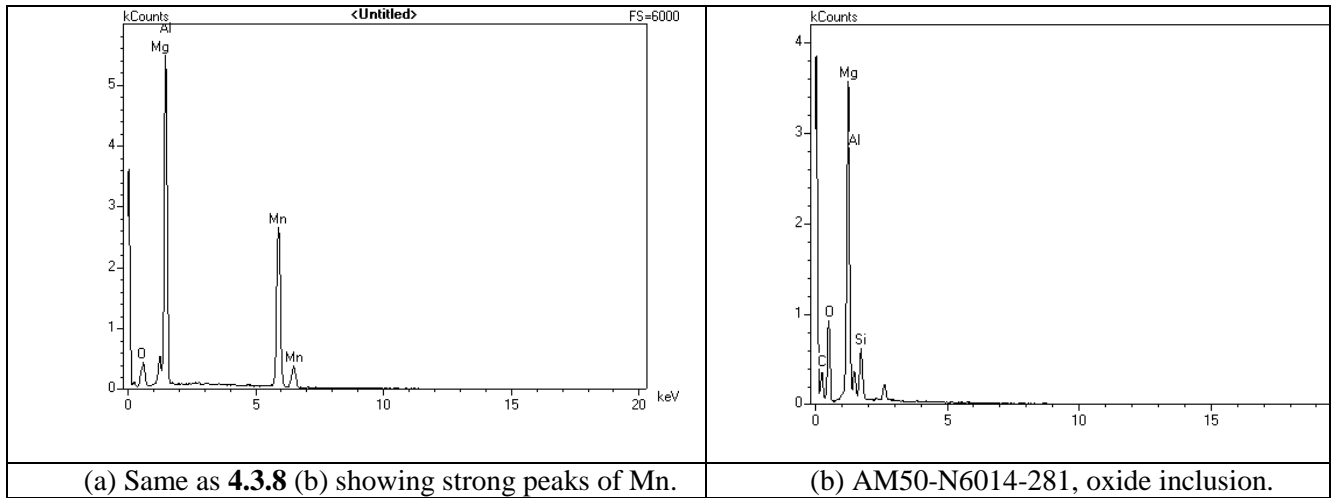


Figure 4.3.9 EDS spectra from AM50 round test bars machined from 24 mm thick plate.

4.3.2.5 Summary and Conclusions

1. Castings should be poured at relatively high temperatures (high metal superheat) to ensure complete filling of the plate castings.
2. X-ray radiography shows that shrinkage and oxide-inclusion defects can be a problem for lost-foam plate castings.
3. It is believed that the types of casting defects observed can be reduced or eliminated by adding grain refiners to the molten magnesium and using steel mesh filters in the gating system during pouring of the castings.
4. There appears to be no strong correlation between mechanical properties and the section thickness of the plate castings. This may be due to the relatively slow cooling rate of the lost-foam casting process.
5. Measurable improvement in tensile properties was observed after heat treatment for all three alloys.
6. Given that there are currently no standard specifications for the mechanical properties of lost-foam cast magnesium alloys AZ91D, AM50, and ZE41A, this result is preliminary and should be followed by more rigorous future study.

Phase II – UAB Casting Trials

TASK 4 Casting Trials at UAB

The key focus of the casting trials at UAB from June 2012 to March 31, 2014 was to evaluate the effects of vacuum assisted pouring (VAP) and solidification under pressure (SUP) during lost foam casting of the hot tear susceptible aluminum alloys 206 and 535.

4.4.1 Phase II: Experimental

The Lost Foam Casting (LFC) process possesses the ability to cast complex parts that could not be produced economically by other processes. Additionally, the LFC process offers design opportunities, cost effectiveness through consolidation of components and significant energy savings. This process has evolved in the past twenty plus years to provide foundries with scrap rates of less than 3 percent on complex parts (cylinder heads, engine blocks, valves, pumps, etc.).

Similar to other casting processes, tensile mechanical properties of lost foam aluminum castings, especially tensile elongation, are degraded by the presence of folds and porosity. Previous work by the Lost Foam Consortium demonstrated a significant improvement in tensile elongation and a reduction in porosity of samples sectioned from an engine block casting poured at low temperatures and a vacuum of -4.5 psig on a 319 and A356 aluminum alloys²⁵. The root cause of folds has been traced to merging metal fronts contaminated with residual pyrolysis products and aluminum oxide^{26, 27}. The occurrence of folds in lost foam castings is usually associated with lower metal temperatures and chaotic mold filling. Lower metal temperatures are usually found in last areas to fill.

Porosity in lost foam aluminum castings can be traced to three major sources – hydrogen gas, solidification shrinkage, and entrapped pyrolysis gases. Hydrogen concentration can be controlled with de-gassing. Porosity formed by pyrolysis gases is usually addressed by coating selection and pouring temperature. Solidification shrinkage can be managed with gating to feed critical areas or with risers if necessary.

Gravity filling generates metal head pressure gradients in relatively large castings and multiple layered castings in the flask. These pressure gradients generate higher metal velocities near the drag surface and lower metal velocities near the cope. This is not a major issue with open cavity processes due to higher overall metal velocities; however, the lower metal velocities in LFC cause significant temperature gradients which affect metal feeding during filling and solidification. Coatings and pouring temperatures are adjusted to minimize casting anomalies that occur in the areas last to fill (lowest temperatures). Anomalies are typically folds, which form when insufficient time is available for the pyrolysis products to exit the casting cavity before solidification. Typically, the foundry solution is higher pouring temperatures. Unfortunately higher pouring temperatures cause three issues that degrade mechanical properties: increased solubility of hydrogen in aluminum; higher metal velocities which generate a higher percent of liquid pyrolysis products²⁸; and increased volumetric shrinkage.

The foregoing discussion indicates a need for a process that allows lower pouring temperatures (to minimize hydrogen porosity and volumetric shrinkage without generating folds), provide for efficient removal of liquid pyrolysis products and minimize the effect of gravity on metal head pressure.

The Vacuum Assisted Pouring (VAP) process fulfills these requirements. First, vacuum applied on the sand/coating side of a Lost Foam cluster provides a more uniform pressure gradient within the flask, allowing metal to be poured at lower temperatures²⁵. This reduces the maximum hydrogen solubility.

Second, metal velocities will increase slightly due to a larger pressure gradient between metal and sand; however, the reduced metal viscosity at lower temperature will offset a major portion of this increase. This increased pressure gradient will increase the pyrolysis product removal rate. The pyrolysis formation and removal is clearly illustrated in the literature. Zhao, Burke and Gustafson³¹ studied the formation of liquid pyrolysis product globules at the metal/coating interface after the metal front had passed. Their research revealed that metal to liquid pyrolysis contact was impossible due to the low boiling temperature of polystyrene (438°C). This indicated that all pyrolysis products must exit the casting cavity as a gas and the escape paths are a gap between the metal and receding pattern during filling and a gap between the metal and liquid pyrolysis globules after the metal front has passed. This is illustrated in Figure 4.4.1. The vacuum applied to the coating will expedite the gas removal.

Third, typical lost foam aluminum castings experience a pressure gradient during filling due to the changing metal head pressure. For example a 20 inch tall casting with a 24 inch tall sprue will experience a metal pressure of about 2.4 psig at the casting bottom and about 0.4 psig at the casting top. These pressures are the driving force that controls metal filling rate and removal of the pattern pyrolysis products from the casting cavity. Typical lost foam castings suffer from increased anomaly severity near the top of the casting where metal velocities and temperatures are lowest. Vacuum Assisted Pouring is a process designed to minimize the effects of changing metal head pressure. For example a -4.5 psig vacuum would be similar to adding an additional 45 inches of sprue height to the casting. Unfortunately, the applied vacuum increases the metal filling velocity, metallostatic pressure, and final metal temperature after filling, increasing the probability of sand burn-on temperatures.

Previously, VAP was used to cast four cylinder engine blocks using A319 alloy²⁵. The following variables were studied:

- Pouring temperatures: 1450°F (788°C), 1350°F (732°C), 1250°F (677°C)
- Pressure: -4.5 psig (9 in. Hg)

Compared to production castings (no vacuum), significant increases in tensile elongation and reductions in fracture surface porosity occurred at a 1250°F (677°C) pouring temperature. Although the increases in elongation were small, they were statistically significant. Tensile elongation values increased from 0.86% (no vacuum) to 1.06% while the fracture surface porosity values decreased from 2.07% (no vacuum) to 0.72%. Based on these results another study was performed, using the same four cylinder block and A356 alloy. The results of this study were similar to the A319 study²⁵.

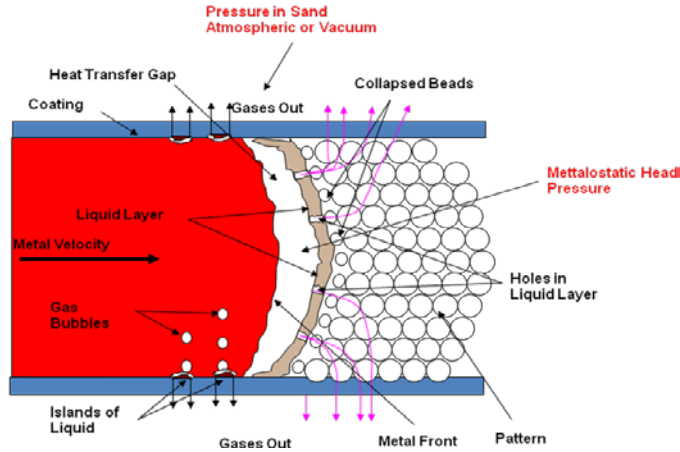


Figure 4.4.1 Lost foam metal filling model.

Metal fill rate and pyrolysis removal rate can be increased by increasing the pressure differential between the metal and sand.

Application of SUP at a pressure of 150 psig (1.03 MPa) on A356 and A206 revealed a significant increase in tensile elongation and ultimate strength^{34, 35}. Solidification under pressure provides two benefits. The applied pressure will push liquid metal through interdendritic regions with a higher solid fraction compared to a conventionally cast part. This will reduce or eliminate solidification shrinkage in marginally fed sections of a casting. Second, hydrogen porosity volume will be reduced to 1/10th (at 150 psig) of an atmospheric pour. The alloy test matrix included a modified 319 (319m), A356, A206 and 535 aluminum. The 319m and A356 are commonly cast using the Lost Foam process and has been examined in the past with SUP and VAP processes. A206 and 535 were included in the alloy test matrix to provide some data on Al-Mg and Al-Cu alloys which typically have higher strength and elongation properties but are prone to hot tearing. Since hot tearing is a solidification issue, the combination of lower temperatures with VAP and improved feeding with SAP may minimize or eliminate this challenge.

4.4.2 Results and Discussion

Figure 4.4.2 shows a schematic of a vacuum assisted pouring apparatus used in previous studies. The flask had a screened chamber in the bottom where vacuum was applied. Figure 4.4.3 shows the actual flask with thermocouple and pressure transducer instrumentation after pouring.

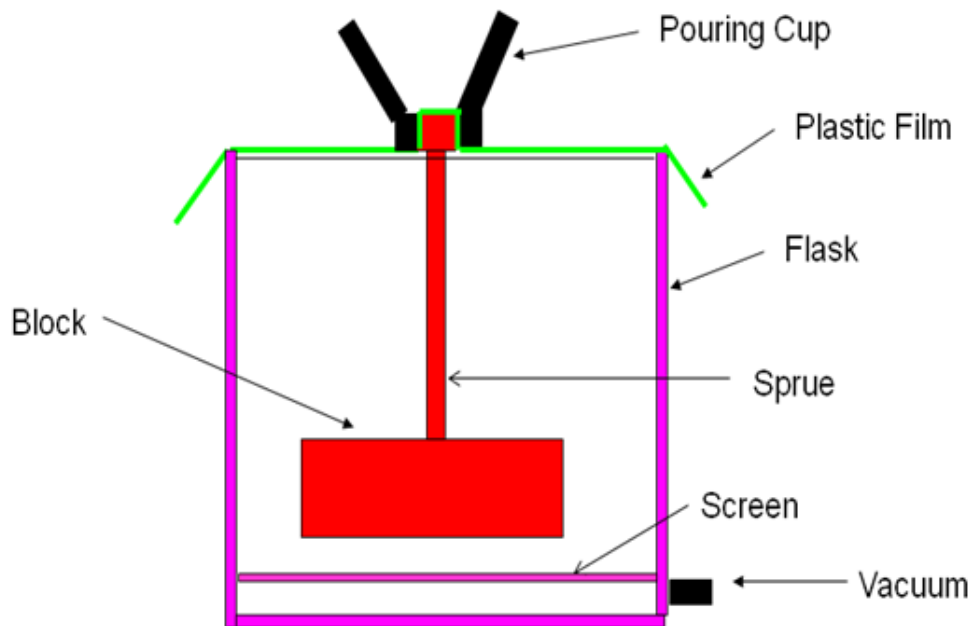


Figure 4.4.2 Vacuum assisted pouring schematic.



Figure 4.4.3 Molding flask, thermocouples, and pressure instrumentation after pouring.

The current study required a change in the flask size and method of applying vacuum since the flask used in previous studies was too large for the pressure vessel. Also the method of applying vacuum was changed. A manifold was designed and constructed. This manifold consisted of steel tubing with multiple holes wrapped with 100 mesh stainless steel screen. The manifold has a vertical tube which

extends above the sand. A flexible hose was clamped on this extension and connected to a 40 HP vacuum pump. Figure 4.4.4 illustrates the flask and vertical vacuum connection positioned inside the pressure vessel.



Figure 4.4.4 Experimental flask and vacuum tube inside pressure vessel.

A top gated four cylinder engine block casting was selected for this study (Figure 4.4.5) in order to rely on the procedures and experience of previous studies¹. This is a production part and will provide direct evidence of any improvement in properties. The part contained sections as thin as 4mm and is a very complex geometry so opportunities exist for hot tearing and incomplete fill. After compacting sand around the cluster, a plastic film was placed over the top of the flask, sprue and vacuum tube. A vacuum hose was connected and a pouring basin was installed, sealing the upper surfaces of the flask and sand. Castings poured and solidified at atmospheric conditions were poured in the normal manner.

Castings poured with vacuum and solidified under pressure were poured inside the pressure vessel as illustrated in Figure 4.4.6. When the casting was filled, the vacuum hose was quickly disconnected, the pressure vessel lid was closed and pressure applied. Both compressed air and nitrogen were used to minimize the time to maximum pressure. The process of removing the vacuum hose and pouring basin, closing the lid and pressurizing the vessel was refined with practice and usually consumed about 120 seconds. Both vacuum and pressure were recorded using a pressure transducer connected to a metal tube placed in the main bearing area. This tube extended through the fittings in the pressure vessel wall.



Figure 4.4.5 Top gated engine block.



Figure 4.4.6 Flask showing pouring basin inside pressure vessel.

Degassing was performed using argon distributed through a rotating graphite tube for at least 30 minutes. Hydrogen content was checked with a reduced pressure test and the heat was degassed until no visible porosity was observed in the test sample. Alloy additions were 0.01% Sr as Al-10%Sr alloy and 0.01% Ti as TiBor (Al-5%Ti-1%B). A 310°F superheat was used for the pouring temperature of all castings poured at atmospheric pressure. A 110°F superheat was used for the pouring temperature of all castings poured with vacuum. Before each pour, a chemistry button was cast and analyzed. Each casting was inspected, followed by sectioning and tensile specimen removal as shown in Figure 4.4.7. Tensile tests were performed using ASTM B 557 procedures³² on a MTS 810 Materials Test System. Two (2) tensile specimens were removed from each of the three main bearing sections, resulting in six (6) tensile

specimens from each block casting. A microstructure/porosity sample was removed from each main bearing.

The test matrix for this study is illustrated in Table 4.4.1 and the compositions of the alloys are shown in Table 4.4.2. A baseline casting was poured and solidified for each alloy at atmospheric pressure and a pouring temperature 310°F above liquidus. A second casting was poured for each alloy using -4.5 psig vacuum and 110°F above liquidus and solidified under a pressure of 150 psig. A deviation from this procedure was used for the A356 alloy in an attempt to separate the effects of vacuum pouring and solidification under pressure (pours AB and C). Casting AB was poured using a vacuum of -4.5 psig and solidified at 0 psig. Casting C was poured with no vacuum and solidified under a pressure of 150 psig.

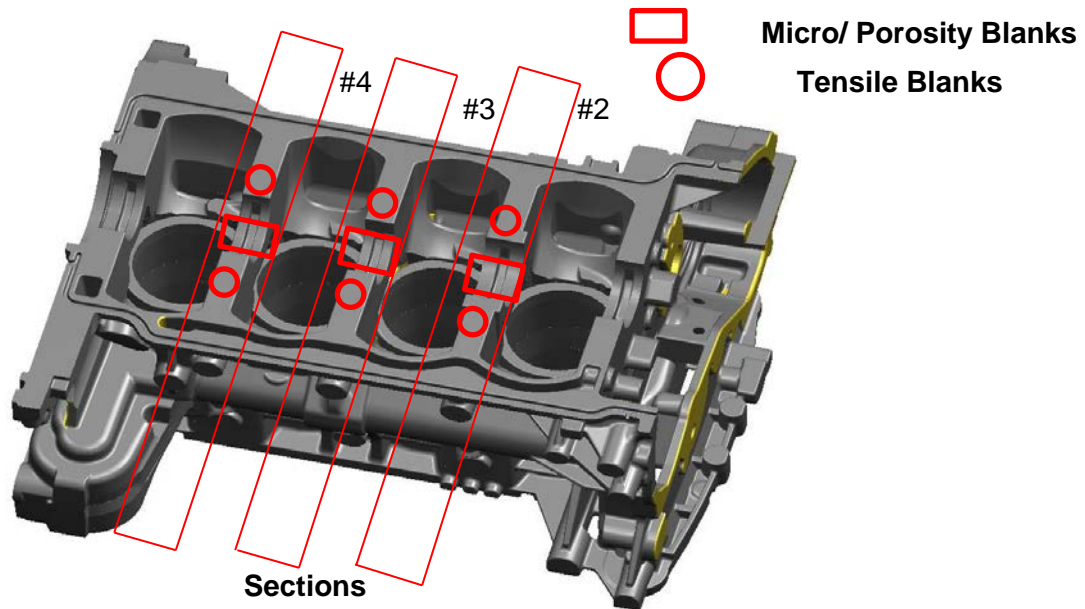


Figure 4.4.7 Engine block showing where test samples were sectioned from.

Table 4.4.1 VAP and SUP test matrix

ID	Alloy	Pour Temperature °F (°C)	Pour Pressure (psig)	Solidification Pressure (psig)
A	A356	1450 (788)	0	0
B	A356	1250 (677)	-4.5	150
AB	A356	1250 (677)	-4.5	0
C	A356	1450 (788)	0	150
D	A206	1510 (821)	0	0
E	A206	1310 (710)	-4.5	150
F	535	1470 (688)	0	0
G	535	1270 (688)	-4.5	150
H	319m	1430 (777)	0	0
J	319m	1230 (666)	-4.5	150

Table 4.4.2 Chemical analysis test matrix alloys

ID	Alloy	Elements, Wt. (%)								
		Si	Fe	Mn	Mg	Cu	Zn	Ti	Sr	B
A	A356	6.92	0.042	0.006	0.341	0.005	0.043	0.163	0.045	0.001
B	A356	6.94	0.157	0.030	0.352	0.053	0.032	0.114	0.019	0.002
AB	A356	6.89	0.121	0.012	0.366	0.008	0.019	0.130	0.028	0.003
C	A356	6.65	0.105	0.011	0.328	0.005	0.018	0.118	0.022	0.002
D	A206	0.24	0.043	0.318	0.322	4.65	0.019	0.178	0.001	0.002
E	A206	0.17	0.042	0.333	0.310	4.66	0.019	0.191	0.001	0.002
F	535	0.42	0.056	0.150	6.97	0.002	0.012	0.165	0.001	0.003
G	535	0.67	0.053	0.160	6.62	0.001	0.001	0.172	0.001	0.003
H	319m	6.68	0.524	0.411	0.549	2.96	0.874	0.132	0.010	0.004
J	319m	6.79	0.536	0.555	0.414	3.32	0.878	0.125	0.009	0.002

Each tensile blank was heat treated prior to machining the tensile specimens. A356 and 319m was given a T6 temper, 535 was tempered to T5 and a T7 temper was given to A206. Ultimate tensile strength and strain at maximum stress were obtained from the stress – strain curves.

Table 4.4.3 summarizes the tensile properties for three main bearing sections of the engine block. In general, the ultimate tensile strengths and elongations of the base line castings (A, D, F and H), poured and solidified at atmospheric conditions, were typical of sand castings³³.

The effect of VAP and SUP on the ultimate tensile strength and strain at maximum stress indicates a general trend of increasing values with the exception of A356 alloy. These results for A356 are similar to results from a previous study where little or no increase in tensile properties occurred. The trends for ultimate strength, strain at maximum stress and porosity is illustrated in Figures 4.4.10 through 4.4.15 for A356, Figures 4.4.16 through 4.4.19 for A206, Figures 4.4.20 through 4.4.23 for 535, and Figures 4.4.24 through 4.4.27 for 319m. The error bars are +/- 1 standard deviation. These results will be discussed separately for each alloy. Table 4.4.4 lists the average and standard deviation values for fracture face porosity.

Table 4.4.3 Average tensile properties from test matrix alloys

ID	Alloy	Pour Temperature °F (°C)	Pressure, psig VAP (SUP)	UTS, ksi	Strain At Max, Stress %
A	A356	1450 (788)	0 (0)	34.1	5.3
B	A356	1250 (677)	-4.5 (150)	36.4	4.7
AB	A356	1250 (677)	-4.5 (0)	35.4	4.5
C	A356	1450 (788)	0 (150)	36.5	6.8
D	A206	1510 (821)	0 (0)	49.8	0.7
E	A206	1310 (710)	-4.5 (150)	56.5	2.2
F	535	1470 (688)	0 (0)	26.4	4.1
G	535	1270 (688)	-4.5 (150)	42.8	16.4
H	319M	1430 (777)	0 (0)	33.5	0.8
J	A319M	1230 (666)	-4.5 (150)	36.9	1.0

Table 4.4.4 Fracture face percent porosity

ID	Alloy	Pour Temperature F (C)	Pressure, psig VAP (SUP)	Avg.	Std. Dev.
A	A356	1450 (788)	0 (0)	4.8	0.90
B	A356	1250 (677)	-4.5 (150)	0.5	0.15
AB	A356	1250 (677)	-4.5 (0)	2.8	1.14
C	A356	1450 (788)	0 (150)	0.2	0.05
D	A206	1510 (821)	0 (0)	14.0	1.7
E	A206	1310 (710)	-4.5 (150)	1.5	0.94
F	535	1470 (688)	0 (0)	5.9	1.27
G	535	1270 (688)	-4.5 (150)	0.6	0.62
H	A319	1430 (777)	0 (0)	8.7	1.8
J	A319	1230 (666)	-4.5 (150)	0.1	0.05

Alloy A356

The tensile results for A356 (Figures 4.4.8 and 4.4.9) indicate little or no effect on strain at maximum stress when VAP and/or SUP was used. Ultimate strength did increase by about 7% from baseline. Fracture face porosity decreased from a baseline of 4.8% to 2.8% when VAP was used, to 0.5% when VAP and SUP was used, and to 0.2% when SUP was used. These results indicate that tensile properties are no longer strictly controlled by porosity but are influenced by other material properties. These results are consistent with a previous study²⁵.

Comparing Figure 4.4.10 to Figure 4.4.11 reveals that VAP significantly reduced the porosity of A356 alloy. Likewise, comparing Figure 4.4.11 to Figure 4.4.12 reveals that VAP and SUP further reduced the porosity. Comparing Figure 4.4.13 to Figure 4.4.12 reveals that SUP alone can achieve similar reductions in porosity compared to VAP and SUP together; however neither of these casting processes significantly improved the tensile properties. These results, although not quantitative, are consistent with the fracture face porosity values listed in Table 4.4.4 and the tensile properties listed in Table 4.4.3.

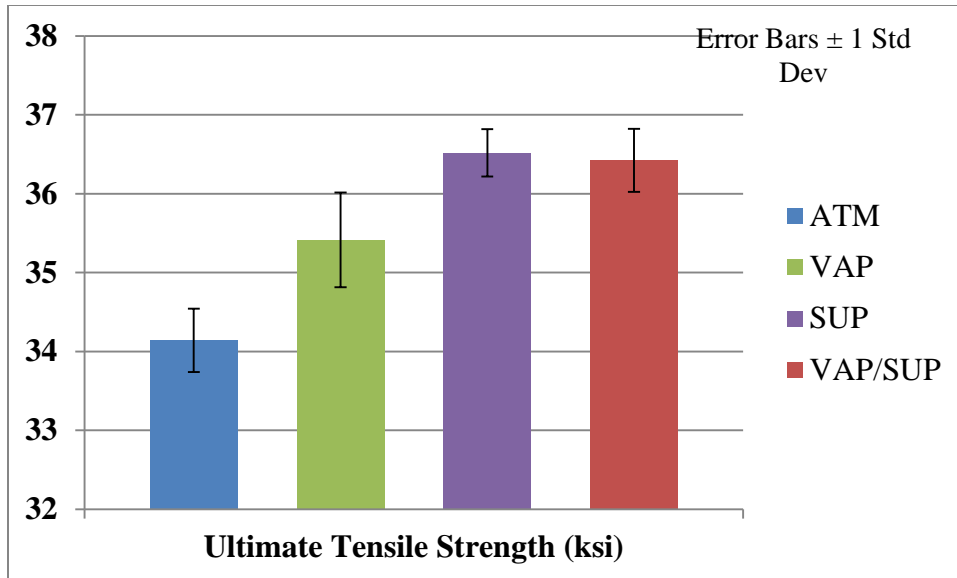


Figure 4.4.8 Effect of VAP and SUP on ultimate strength for alloy A356.

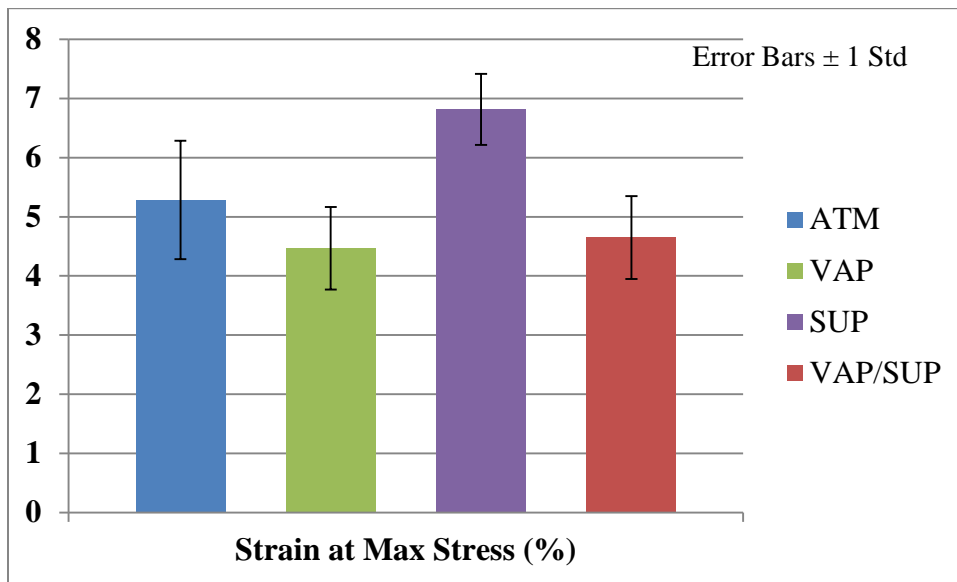


Figure 4.4.9 Effect of VAP and SUP on strain at maximum stress for alloy A356.

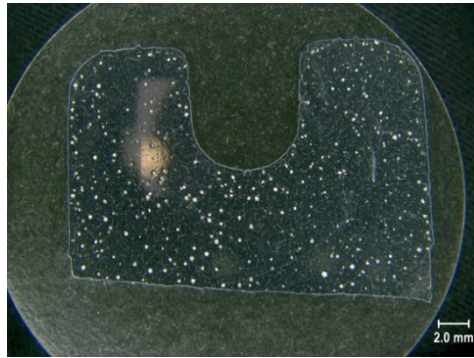


Figure 4.4.10 Porosity of Casting A, A356, 1450°F, VAP (0 psig) and SUP (0 psig), Bearing #4.

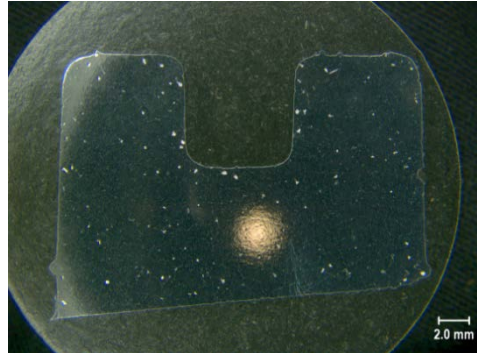


Figure 4.4.11 Porosity of Casting AB, A356, 1250°F, VAP (-4.5 psig) and SUP (0 psig), Bearing #4.



Figure 4.4.12 Porosity of Casting B, A356, 1250°F, VAP (-4.5 psig) and SUP (150 psig), Bearing #4.



Figure 4.4.13 Porosity of Casting C, A356, 1450°F, VAP (0 psig) and SUP (150 psig), Bearing #4.

Alloy A206

A206 has a longer solidification range compared to A356 which increases the likelihood of both hot tearing and solidification shrinkage. Figures 4.4.15 and 4.4.16 indicates that an increase in ultimate tensile strength and strain at maximum stress can be achieved for A206 alloy using VAP and SUP. Ultimate strength increased by 10% from 50 to 55 ksi and maximum strain increased 300% from 0.7% to 2.2% with the application of VAP and SUP.

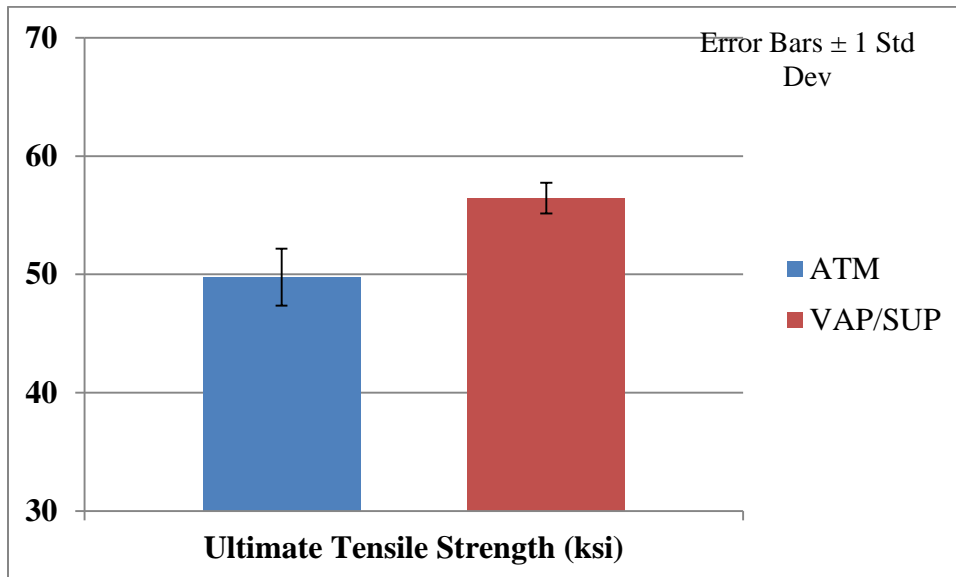


Figure 4.4.14 Effect of VAP/SUP on ultimate strength for alloy A206.

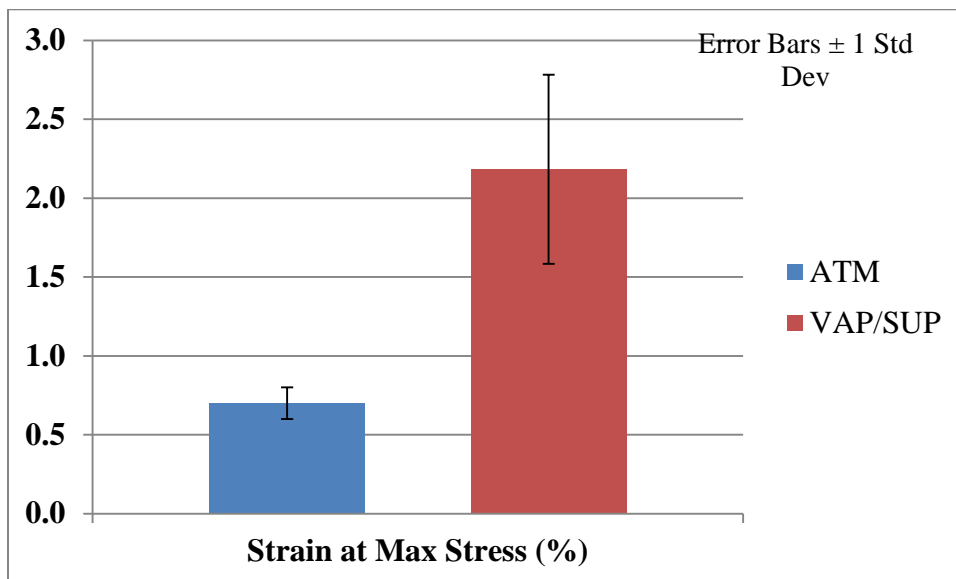


Figure 4.4.15 Effect of VAP/SUP on strain at maximum stress for alloy A206.

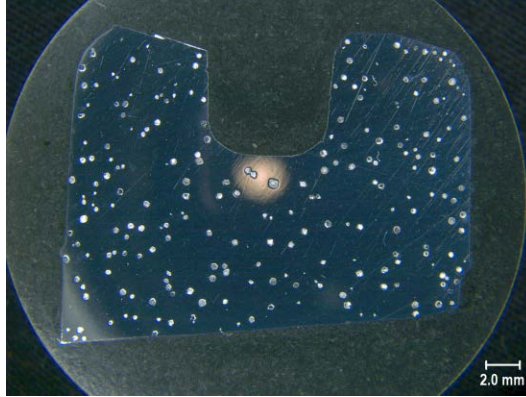


Figure 4.4.16 Porosity of Casting D, A206, 1510°F, VAP (0 psig) and SUP (0 psig), Bearing #4.

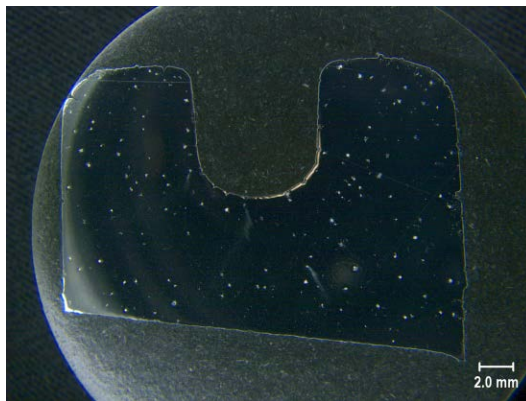


Figure 4.4.17 Porosity of Casting E, A206, 1310°F, VAP (-4.5 psig) and SUP (150 psig), Bearing #4

Comparing Figure 4.4.16 to Figure 4.4.17 reveals a visual decrease in porosity for A206 using the VAP/SUP casting process. Quantified values of fracture face porosity in Table 4.4.3 confirm these visual observations. However, A206 had the highest fracture surface porosity baseline (14%). Even though VAP/SUP reduced fracture surface porosity to 10% of baseline, the 1.5% value was the highest VAP/SUP value of the four alloys examined. On average, VAP/SUP reduced fracture surface porosity to 1/10th of the baseline value for all alloys examined.

Alloy 535

VAP/SUP increased ultimate strength from 25 to 42 ksi compared to the baseline value as illustrated in Figure 4.4.18. Strain at maximum stress also increased significantly from 4% to 16% (Figure 4.4.19). The fracture face porosity for 535 alloy was reduced from 5.9% to 0.6% when VAP and SUP was used for the casting process. Comparison of the metallurgical porosity content in the conventionally cast bearing journal (Figure 4.4.20) to the VAP/SUP cast journal (Figure 4.4.21) showed a dramatic reduction in porosity. Improved tensile properties reflected this porosity decrease.

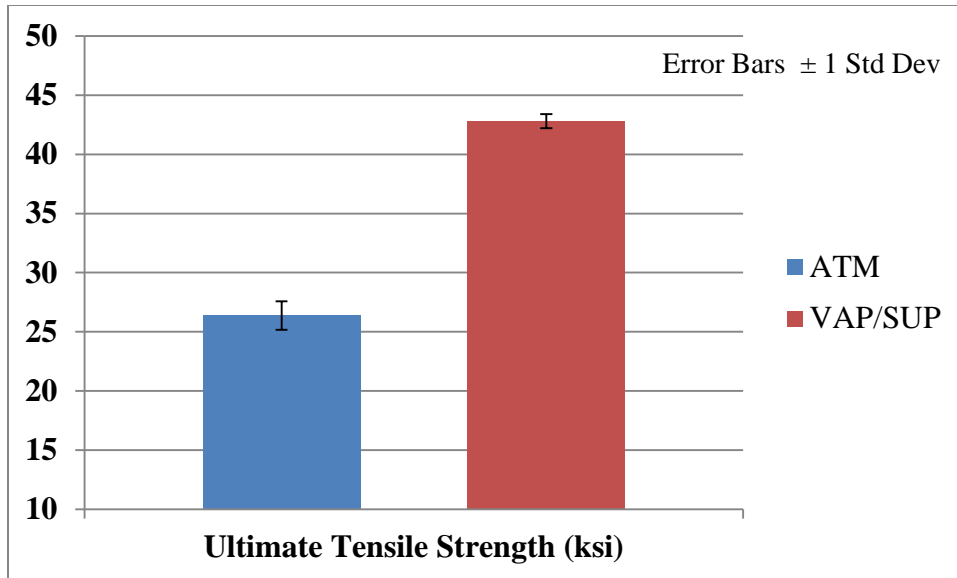


Figure 4.4.18 Effect of VAP/SUP on ultimate strength for alloy 535.

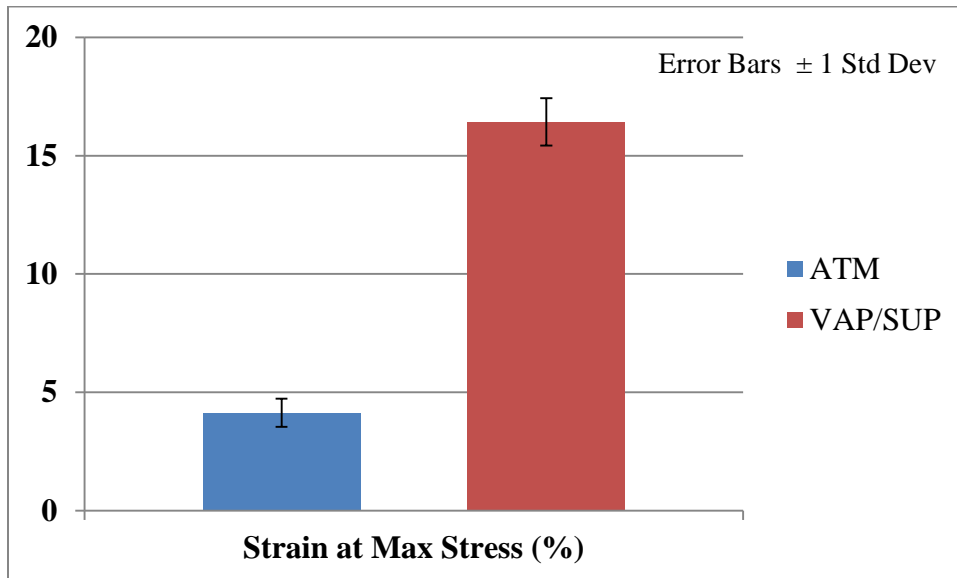


Figure 4.4.19 Effect of VAP/SUP on strain at maximum stress for alloy 535.



Figure 4.4.20 Porosity of Casting F, 535, 1470°F, VAP (0 psig) and SUP (0 psig), Bearing #4.

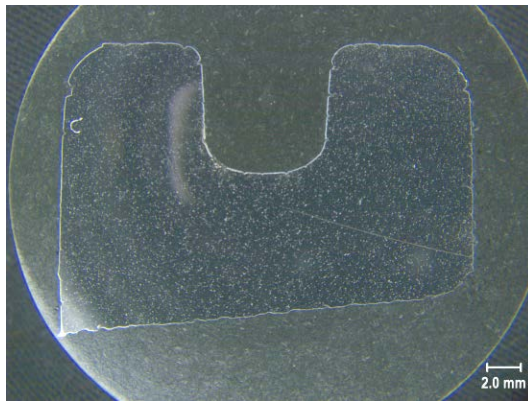


Figure 4.4.21 Porosity of Casting G, 535, 1270°F, VAP (-4.5 psig) and SUP (150 psig), Bearing #4.

Alloy 319m (modified)

Although not large, a significant increase in tensile ultimate strength resulted from the porosity decrease (Figure 4.4.22). No significant increase in strain at maximum stress was evident (Figure 4.4.23). This is indicative of other factor(s) controlling tensile properties. VAP/SUP application significantly reduced the quantity and size of porosity for 319m alloy (Figures 4.4.24 and 4.4. 25).

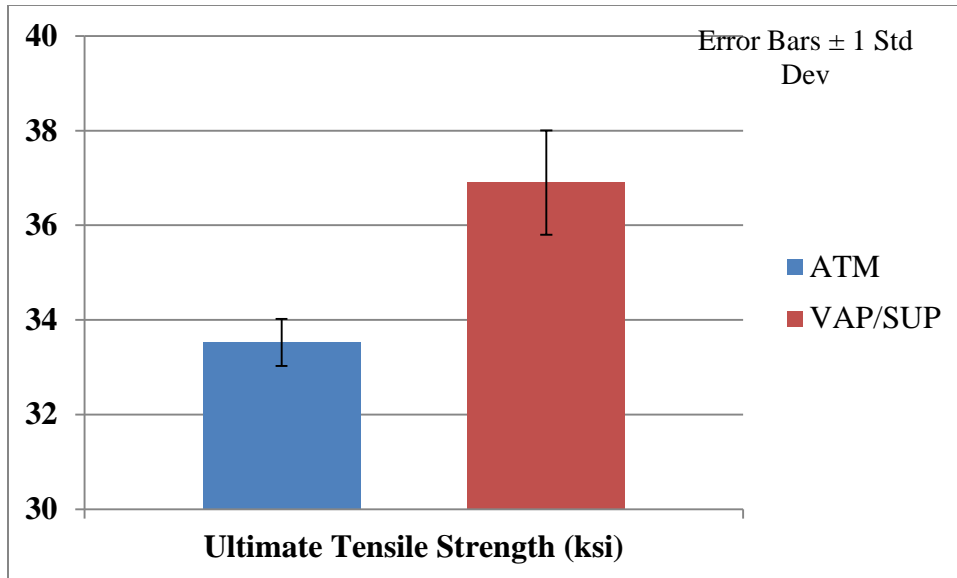


Figure 4.4.22 Effect of VAP/SUP on ultimate strength for alloy 319m.

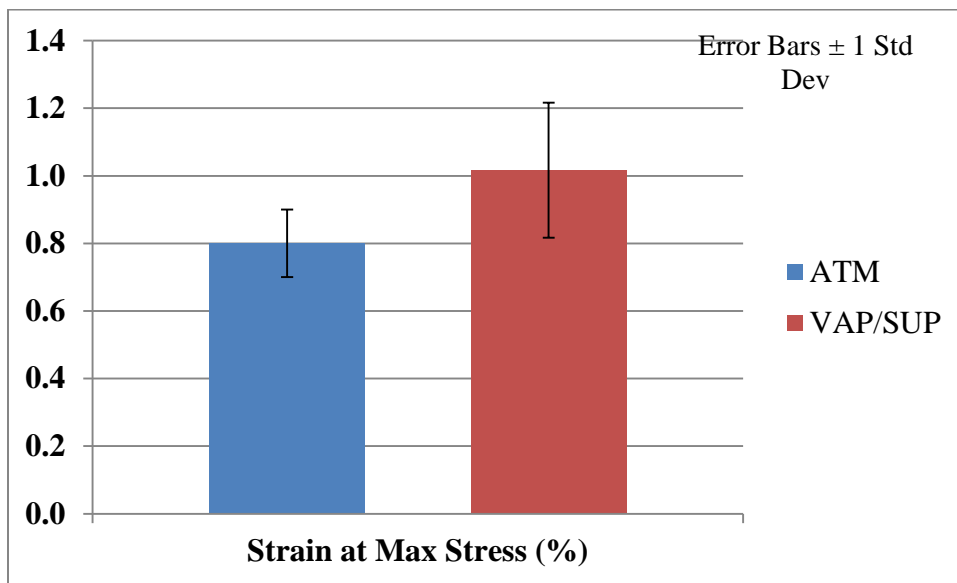


Figure 4.4.23 Effect of VAP/SUP on strain at maximum stress for alloy 319m.



Figure 4.4.24 Porosity of Casting H, 319m, 1430°F, VAP (0 psig) and SUP (0psig), Bearing #4.

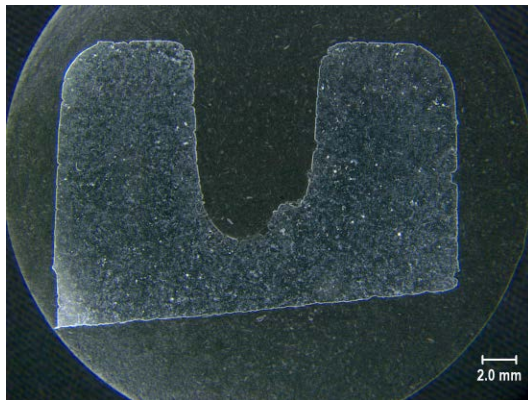


Figure 4.4.25 Porosity of Casting J, 319m, 1230°F, VAP (-4.5 psig) and SUP (150 psig), Bearing #4.

A visual examination of each cast block has been conducted to detect any surface imperfections such as hot tearing or cracks. No cracks or hot tearing were detected although surface suck-in was observed the conventionally cast 535 block. The location of the suck-in was at a hot spot located near the deck face. Since hot tears and cracks are most likely to form at hotspots, solidification modeling of the block will be performed to identify areas for further examination.

5 Benefits Assessment

5.1 Casting Trials at CMAT

Significant energy savings can be achieved with improved casting yield, reduced hot tearing, ability to cast thinner walls, use of un-bonded sand and part consolidation as the foam pattern can be glued together to produce complex shapes leading to reduced machining costs. In specific terms, it may be possible that 25% of Al-Mg (e.g. 535) and Al-Cu (e.g. 206) alloys currently poured in sand mold can be converted into lost foam casting, and that up to 50 % of Mg (e.g. AM50, AZ91E) alloys can be poured using lost foam process. The energy savings that can be achieved from this project are as follows: By using un-bonded molding sand and reduced finishing cost of castings. From improved casting yield, about 65% with lost foam casting compared with about 50% or less for regular sand castings, (less metal to be re-melted) with lost foam. Elimination of binder and energy required for sand mixing. By using alloys 206 higher tensile properties can lead to reduced section thickness and weight. Alloy 535 it exhibits good mechanical properties and dimensional stability in the as-cast condition, when heat-treated, a T5 heat treatment, instead of T6 commonly used for alloy A356 can be used.

5.2 Casting Trials at UAB

With the increased emphasis on vehicle weight reduction, production of near-net shape components by lost foam casting will make significant inroad into the next-generation of engineering component designs. Lost foam casting process is a cost effective method for producing complex castings using an expandable polystyrene pattern and un-bonded sand. Some of the unique advantages of using lost foam casting process are closer dimensional tolerance, higher casting yield, and the elimination of sand cores and binders. Most of the aluminium alloys poured using the lost foam process are based on the Al-Si system. Very limited work has been done with Al-Mg and Al-Cu type alloys. Significant weight savings can be achieved by casting thin-wall (≤ 3 mm) engineering components from these higher strength aluminum-base alloys.

The Lost Foam Casting (LFC) process possesses the ability to cast complex parts that could not be produced economically by other processes. Additionally, the LFC process offers design opportunities, cost effectiveness through consolidation of components and significant energy savings. This process has evolved in the past twenty plus years to provide foundries with scrap rates of less than 3 percent on complex parts (cylinder heads, engine blocks, valves, pumps, etc.).

The potential energy savings at pouring temperatures of 1250°F (677°C) compared to 1450°F (788°C) are very large. The estimated savings for this temperature reduction is 17 - 19%²⁹. In addition, CO₂ emissions would be significantly reduced³⁰ and melting and holding furnace life would be extended. Furthermore, the use of non-traditional higher strength aluminum alloys would allow designers to produce either lighter weight components at current stress levels or higher performance parts at current part weight. This would provide significant indirect energy savings and CO₂ emission reduction.

6 Commercialization

6.1 Casting Trials at CMAT

Currently, there is no commercial foundry in North America that is dedicated to the lost foam casting of magnesium alloys. It was demonstrated that the vacuum application technique resulted in improved mold filling, extraction of mold gasses, casting of near-net-shape and thin wall components, and reduced casting defects. The casting of three prototype components (ELX body, Intake Manifold, and Widget) successfully from three magnesium alloys is indicative of possible commercial viability of the casting process developed. This research outcome opens an opportunity to produce cast components such as an automotive engine block from some of the new high temperature magnesium alloys that are susceptible to hot cracking when poured in metal molds. With additional research and development efforts lost foam casting of magnesium alloys for automotive and other applications where significant weight savings is required can become a reality.

Some unique advantages of the LFC process are close dimensional tolerance, part consolidation, high casting yield, capability to produce complex castings, and elimination of sand cores and binders. The flexibility of gluing foam sections together to form one component with complex internal passages – as in engine blocks and heads – without the use of cores common in the sand-casting process is one of the major advantages of the LFC process. Some automotive engine blocks and heads are cast from aluminum alloy A356 using the LFC process. It is quite possible that some of the new magnesium alloys developed for high-temperature applications could be used in the same way with further reduction in vehicle weight and improvement in fuel economy.

The engine block is the heaviest single component of an engine, and by using magnesium engine block and other powertrain components produced by the LFC process, significant weight reduction and improved fuel economy can be achieved. For example, the BMW's 3.0 litre Mg/Al composite engine block produced by high pressure die-casting process weighs about 24% less than an Al block. Some of the unique advantages of the LFC process are the production of complex and near-net-shape components, and elimination of sand binders and cores, leading to reduced (GHG) emissions.

6.2 Casting Trials at UAB

This project has given quarterly status reports and has directly interacted with the American Foundry Society (AFS) Division 11 committee (Lost Foam Committee). In addition, a presentation will be given and a paper has been submitted for the 2014 AFS Congress in April 2014. Furthermore, an aluminum lost foam foundry has expressed an interest in VAP as a potential remedy to a filling defect that is a major contributor to their scrap rate. As lost foam section thicknesses become thinner to reduce weight, filling sections with glue joints becomes a challenge. The glue, which has a much higher density than foam, requires a certain amount of energy to decompose or a through wall leaker can develop. While the incidence of leakers may be relatively low, the foundry must perform post-processing to identify and plug the leak. VAP reduces the pour time which should provide a more uniform metal temperature throughout the casting. And the vacuum should reduce the decomposition gas pressure of the glue, minimizing the metal front delay. With the aid of the foundry, UAB will inspect the test casting to determine if these leakers are less prevalent in VAP castings compared to conventionally poured castings. While the data population will be too small to be definitive, it may provide enough useful information for further investigation by the foundry.

7 Accomplishments

7.1 Casting Trials at CMAT

7.1.1 Innovative Processing Techniques

Innovative processing techniques were developed and six journal and conference proceeding publications from the outcome of completed tasks. The technical and processing challenges associated with the lost foam casting of magnesium alloys are related to its high reactivity, low heat content, and low density.

It was demonstrated in that the processing techniques used for aluminum alloys were not adequate for magnesium alloys. The developed novel processing technology is a significant breakthrough and offered new manufacturing route for magnesium engine block and other power train components. The casting trials show that lost-foam casting process can be a viable manufacturing route for magnesium alloys AZ91D/E, AM50 and ZE41A. The development of novel processing techniques such as the using of:

- Carboceramic backing sand instead of silica sand (because it does not react with molten magnesium when un-inhibited);
- Lower density foam patterns and foam coating material (to reduce foam decomposition products);
- Hollow pyrolite fiber sprue (to improve mold filling); and
- Vacuum during molding and pouring (to improve the packing of the sand around the foam pattern and improved extraction of mold gasses).

7.1.2. Publications

1. Fasoyinu, F. A., and Sahoo, Mahi., "Lost Foam Casting of Selected Magnesium Alloys", MTL 200911(CF), 56 pages.
 2. Fasoyinu, Yemi., and Sahoo, Mahi., "Lost Foam Casting of Magnesium Alloys for Automotive Applications", International Foundry Research / Giessereiforschung 59 (2007) No. 4, pp. 2-15 (2007).
 3. Fasoyinu, Yemi., and Sahoo, Mahi., "Lost Foam Casting of Magnesium Alloys for Automotive Applications", published in the Proceeding of 64th IMA World Congress, Vancouver, B.C. Canada. May 13-15, 2007.
 4. Fasoyinu, Y., Newcombe, P., and Sahoo, Mahi., "Lost Foam Casting of Magnesium Alloys AZ91D and AM50", AFS Transactions, Vol. 114, (2006), pp.
 5. Fasoyinu, Yemi., Newcombe, Peter., Nolan, Dennis., and Sahoo, Mahi., "Development of Lost Foam Casting Technology for Magnesium Alloys", Proceeding of Lost Foam 2006 Conference, Paderborn, Germany, October 11-12, 2006.
 6. Fasoyinu, Yemi., Chiorean, Horatiu., Newcombe, Peter., and Sahoo, Mahi., "Vacuum Assisted Lost Foam Casting of Magnesium Alloy AZ91E", AFS Transactions, Vol. 113, (2005).
-

7.2 Casting Trials at UAB

This project has demonstrated that net shape thin walled engineering components can be successfully cast from aluminum alloys A356, A206, 535 and modified alloy 319 at 110°F (43°C) above liquidus temperatures using the VAP process. This pouring temperature is significantly less than typical temperatures used in lost foam foundries. This results in significant energy savings and extends melting and holding furnace life.

The Al-Si alloys (A356 and 319m) Al-Cu alloy (A206) and showed some, but not dramatic improvement in tensile properties with VAP/SUP, even when fracture surface porosity was reduced to 10% of baseline. This would indicate that other metallurgical factor(s) were dominate or optimization of the melting practice and VAP/SUP processing may give better results. The Al-Mg alloy (535) showed the most dramatic improvements in tensile properties, a 70% increase in ultimate strength and 300% increase in strain at maximum stress.

All castings were examined to detect any indications of hot tearing or incomplete fill. Only one instance of suck-in shrinkage was observed in one of the baseline castings. Even the baseline castings did not hot tear with A206 or 535 alloy. The unbonded sand used in the Lost Foam process may provide enough elasticity to minimize hot tear inducing strain during solidification.

7.2.1 Publications

1. H. E. Littleton, J.A. Griffin, and R.D. Foley , "Effect of Vacuum Assisted Filling and Solidification Under Pressure of A356, A206, Modified 319 and 535 Aluminum Alloys on Tensile Properties Using the Lost Foam Casting Process" 2014 AFS Casting Congress, April 2014, Paper 14-071

8 Conclusions (CMAT and UAB)

8.1 CMAT

1. The casting trials demonstrated that lost-foam casting process can be a viable manufacturing route for prototype components poured from magnesium alloys AZ91D/E, AM50 and ZE41A. Given the low heat content of magnesium alloys, castings should be poured with adequate metal superheat to ensure complete filling and degradation of the foam pattern.
2. The use of innovative processing techniques such as: carboceramic backing sand instead of silica sand that does not react with molten magnesium when un-inhibited; lower density foam patterns to reduce foam decomposition products; hollow pyrolite fiber sprue to improve mold filling; and application of vacuum during molding and pouring techniques to improve the packing of the sand around the foam pattern and improved extraction of mold gasses.
3. Based on the degree of mold filling, misruns, and surface finish, the best castings were produced using the Probead 70 foam pattern, and the worst from the Brominated EPS pattern. Further study is required to gain a better understanding when different magnesium alloys are produced.
4. The use of hollow sprue improved mold filling of the widget patterns.

5. From the results of the four coatings evaluated, Styromol 169.23 produced the most complete castings with good surface finish and the sharpest features. These results seem to suggest that the use of high pouring temperature and Styromol 169.23 coating is a good combination for Mg alloy AZ91D.
6. The application of -40 kPa (-6 psi) vacuum is very beneficial to complete mold filling of the wicket, box, and plate patterns in alloy AM50 with 100°C or 140°C superheat.
7. X-ray radiography shows that shrinkage and oxide-inclusion defects can be a problem in cast components from magnesium alloys.
8. Given that there are currently no standard specifications for the mechanical properties of lost-foam cast magnesium alloys AZ91D, AM50, and ZE41A, the results from this study is very preliminary and should be followed by more rigorous future study.

8.2 UAB

1. This project has demonstrated that net shape thin walled engineering components can be successfully cast with A356, A206, 535 and modified 319 aluminum alloys at 110°F (43°C) above liquidus temperatures using the VAP process.
2. The Al-Si alloys (A356 and 319m) showed some, but not dramatic improvement in tensile properties with VAP/SUP, even when fracture surface porosity was reduced to 10% of baseline. This would indicate that other metallurgical factor(s) were dominant.
3. The Al-Cu alloy (A206) also showed some, but not dramatic improvement in tensile properties with VAP/SUP, even when fracture surface porosity was reduced to 10% of baseline. However, the baseline and VAP/SUP fracture surface porosity were the highest values of the four alloys. Optimization of the melting practice and VAP/SUP processing may give better results and should be pursued since the upside with A206 is significant.
4. The Al-Mg alloy (535) showed the most dramatic improvements in tensile properties, a 70% increase in ultimate strength and 400% increase in strain at maximum stress.
5. All castings were examined to detect any indications of hot tearing or incomplete fill. Only one instance of suck-in shrinkage was observed in one of the baseline castings. Even the baseline castings did not hot tear with A206 or 535 alloy. The unbonded sand used in the Lost Foam process may provide enough elasticity to minimize hot tear inducing strain during solidification.

9 Recommendations (CMAT and UAB)

9.1 CMAT

Currently, there is no commercial foundry in North America dedicated to lost foam casting of magnesium alloys. However, a few foundries are specialized in pouring of magnesium alloys used in aerospace applications. Some unique advantages of lost foam casting process are close dimensional tolerance, part consolidation, high casting yield, capability to produce complex castings, and elimination of sand cores and binders. The flexibility of gluing foam sections together to form one component with complex internal passages – as in engine blocks and heads – without the use of cores common in the sand-casting

process is one of the major advantages of lost foam casting process. These sand casting foundries could be approached to take a close look at the design freedom offered by lost foam casting and also consider the added advantage of vacuum application during molding and pouring operations.

9.2 UAB

This project had a very limited scope to fit within the time and financial constraints. But it has demonstrated that the combination of VAP and SUP can produce significant improvements in actual part tensile properties. Current lost foam engineering models for filling and solidification do not incorporate either VAP or SUP into the calculations. For these processes to gain wider acceptance to designers, engineering models must account for the effects of VAP and SUP and verify the modelling results to actual data.

10 References (CMAT and UAB)

1. Dion, J. L., Warda, R.D., Buhr R.K., Emmett J. R. and Sahoo, M. "Production of Aluminum Alloy Castings Using Evaporative Pattern and Vacuum Techniques", AFS Transactions, Vol. 1990, p.131-140.
2. Dion, J. L., and Sahoo, M. "Vacuum Casting of Aluminum Alloys", MTL Report 91-31 (OP-J), 1991, 18 pages.
3. Dion, J. L., Buhr R.K and Sahoo, M. "Vacuum Pouring", MTL Report 90-21 (OP-J), 1990, 14 pages.
4. Sahoo, M., Dion, J. L., Emmett, J.R., and Cousineau, D. "Production of Automotive Castings For GM's Casting Development Laboratory Using Evaporative Pattern and Vacuum", MTL Report # 90-5 (CF), May 1990. 21pages.
5. Blackburn, R. D. "Vacuum Casting Goes Commercial", Advanced Material and Processes, February, 1990, p.17-21.
6. Cook, J. "Vacuum Casting Opens up Design Possibilities", Canadian Machinery and Metal Working, August, 1990, p.16.
7. Thomas, S. P. "CWC Textron Invests in the Promise of advanced Vacuum Casting", Modern Casting, December, 1990, p.22-25.
8. Wang, C., Ramsay, C.W., and Askeland, D.R., "Processing Variables Significance on Filling Thin Plates in the Lost Foam Casting Process: The Staggered Nested Factorial Experiment", AFS Trans, Vol. 105, 1997, pp. 427-434.
9. Liu, J., Askeland, D.R., and Ramsay, C.W., "A Study of the Foam-Metal-Coating Interaction in the Lost Foam Casting Process", AFS Trans, Vol. 105, 1997, pp. 419-425.
10. Hill, M., Lawrence, M., Ramsay, C.W., and Askeland, D.R. "Influence of Gating and Other Processing Parameters on Mold Filling in the Lost Foam Casting Process", AFS Trans, Vol. 105, 1997, pp. 443-450.

11. Lawrence, M.D., Ramsay, C.W., and Askeland, D.R. "Some Observations and Principles for Gating of lost Foam Castings", AFS Trans, Vol. 106, 1998, pp. 349-356.
12. Liu, J, Askeland, D.R., and Ramsay, C.W., "Effect of Foam Density and Density Gradients on Metal Fill in the Lost Foam Casting Process", AFS Trans, Vol. 105, 1997, pp. 435-442.
13. Bennett, S., Ramsay, C.W., and Askeland, D.R. "Temperature Gradients during Fill and Solidification of Lost Foam Aluminum Castings", AFS Trans, Vol. 106, 1998, pp. 357-363, 1998.
14. Hill, H., Vrieze, A., Moody, T., Ramsay, C. W. and Askeland, D. R. "Effect of Metal Velocity on Defect Formation in Aluminum Lost Foam Castings", AFS Preprint 98-114.
15. Marlatt, M., Weiss, D. J. and Hryn, J.N. "Developments in Lost Foam Casting of Magnesium", AFS Transactions, Vol. 111, 8 pages, 2003.
16. Shroyer, H.F. "Cavityless Casting Mould and Method of Making Same", US Patent #2830343, April 15, 1958.
17. Staff Report, "Engine Design Freedom with Lost Foam Casting", Engineered Casting Solutions, Vol. 6, No. 4, 2004, pp. 28-32.
18. Wanliang, S., Littleton, H.E., and Bates, C.E. "Advanced Lost Foam Casting Technology", Report No. 527985-2004, Final Report, Phase V, Submitted the US Department of Energy (DoE), The American Foundry Society (AFS), and AFS-DOE-LFC Foam Casting Consortium Members, February 2005, 54 pages.
19. Jereza, K., Brindle, R., Williams, G., and Chappell, J. "Magnesium Casting Industry Technology Roadmap", Sponsored by American Foundry Society, published by Energetics Inc., Columbia, Maryland, USA, September 2005, 36 pages.
20. Fasoyinu, Y., and Sahoo, M. "Lost Foam Casting of Magnesium Alloys for Automotive Applications", published in the Proceeding of 64th IMA World Congress, Vancouver, B.C., Canada, May 13-15, 2007.
21. ASM Specialty Handbook, Magnesium and Magnesium Alloys, Edited by Michael M. Avedesian and Hugh Baker, published by ASM International, 1993, p. 79, 231.
22. ASM Handbook, 8th Edition, Vol. 7 "Atlas of Microstructures of Industrial Alloys", published by ASM International, 1972, p. 306.
23. Fasoyinu, Y., Chioren, H., Newcombe, P., and Sahoo, M. "Vacuum Assisted Lost Foam Casting of Magnesium Alloy AZ91E", AFS Trans, Vol. 112, 2004.
24. Fasoyinu, Y., Newcombe, P., and Sahoo, M. "Lost Foam Casting of Magnesium Alloys AZ91D and AM50", AFS Trans, Vol. 114, 2006.
25. Littleton, H. E. and Druschitz, Alan "Vacuum Assisted Filling of Lost Foam Castings", AFS Transactions, Paper #10-062 (2010).
26. Zhao, Qi., Gustafson, Thomas W., Hoover, Mark., Flemings, Merton C. "Fold Formation in the Lost Foam Aluminum Process", TMS Annual Meeting (2003), pp. 121-132.

27. Sun, Wanliang., and Littleton, H. E. "Effects of Foam Pattern Fusion on the Quality of Lost Foam Castings", AFS Transactions, Paper #03-083 (2003), pages 1245 -1253.
28. Molibog, Taras., "Experimental Modeling of the Metal/Pattern Exchange Mechanism in the Lost Foam Process", University of Alabama at Birmingham Master's Thesis (1999).
29. Eppich, R and Naranjo, R. D., "Implementation of Metal Casting Best Practices," dor ITP Metal Casting, U. S. Department of Energy (2007).
30. Schifo, J. F. and Radia, J. T., "Potential Impact of CO2 Regulations on Metalcasting Facilities," presentation to the American Foundry Society GHG Adhoc Committee (2008).
31. Zhao, Qi., Burke, John T. and Gustafson, Thomas W. "Foam Removal Mechanism in Aluminum Lost Foam Casting", AFS Transactions, Paper #02-083 (2002).
32. ASTM B557-10, "Standard Test Methods of Tension Testing Wrought and Cast Aluminum and Magnesium Alloy Products," Annual Book of ASTM Standards, Vol. 02.02, ASTM International, West Conshohocken, PA (2002) pp. 406-420.
33. Donahue, Ray., "Quality Control of Aluminum Lost Foam Castings", Lost Foam Sponsors Meeting, June 2005.
34. Chintalapati, P. P., Griffin., J.A., Griffin, R.D., "Effect of Applied Isostatic Pressure during Solidification on the Microstructure and Mechanical Properties of Aluminum Alloy 206", AFS Transactions, Paper #08-079 (2008), pages 169 -183.
35. Chintalapati, P. P., Griffin., J.A., Griffin, R.D., "Improved Mechanical Properties of Lost Foam Cast A356 and A319 Aluminum Solidified under Pressure", AFS Transactions, Paper #07-058 (2007).